Seasonal upwelling–dust controls on export production in the Canary Current System revealed by Lagrangian particle tracking

Catarina V. Guerreiro[1,2,3], Bror F. Jonsson[4], Peter Land[5], Javier Arístegui[6], Jan-Berend Stuut[7,8], Afonso Ferreira[1,2], Gavin H. Tilstone[5], Vanda Brotas[1,2], Steve B. Groom[5]

[1] Marine and Environmental Science Centre (MARE) / Aquatic Research Network (ARNET), Lisbon, 1749-016, Portugal
[2] Departmento de Biologia, Faculdade de Ciências, Universidade de Lisboa (CIÊNCIAS ULisboa), Lisbon, 1749-016, Portugal
[3] Instituto Dom Luiz (IDL), Universidade de Lisboa, Lisbon, 1749-016, Portugal
[4] University of New Hampshire, Durham, NH 03824, USA
[5] Plymouth Marine Laboratory (PML), Plymouth, PL1 3DH, United Kingdom
[6] University of Las Palmas de Gran Canaria, Las Palmas de Gran Canaria, 35001, Spain
[7] Royal Netherlands Institute for Sea Research (NIOZ), Den Burg (Texel), 1790 AB, The Netherlands.
[8] Faculty of Earth and Life Sciences, Vrije Universiteit (VU), Amsterdam, 1081 HV, The Netherlands.

Correspondence to: Catarina V. Guerreiro (cataguerreiro@ciencias.ulisboa.pt)

Abstract. The Canary Current System (CCS) is a major eastern boundary upwelling system where intense nearshore productivity, dynamic offshore transport, and Saharan dust deposition jointly shape biogeochemical cycling. Understanding how these physical and atmospheric forcings regulate particulate export is crucial for assessing the biological carbon pump under ongoing North Atlantic warming.

Here we combine Lagrangian backtracking of satellite-derived chlorophyll-*a* (Chl-*a*), particulate inorganic carbon (PIC), and primary production (PP) with one year of sediment trap fluxes of coccolith species, biogenic particles and lithogenic material (proxy for aeolian dust fluxes) from moorings CB (21ºN, 20ºW) and M1 (12ºN, 23ºW), representing distinct open-ocean settings offshore of NW Africa. These fluxes are further integrated with data from satellite-derived upwelling indices, sea surface height (SSH), aerosol optical depth (AOD), and *in situ* water-column observations collected at the trap locations.

The results reveal strong seasonal connectivity between coastal upwelling, offshore transport, and deep export. Late winter–spring intensification of mixing, upwelling, and filament/eddy activity sustained elevated Chl-*a*, PP, PIC, and high $CaCO_3$ fluxes, with sinking assemblages dominated by fast-blooming (r-selected) placolith-bearing coccolithophores—especially at CB. Lagrangian trajectories further show that this connectivity weakens offshore, with strong coast-to-open-ocean declines in Chl-*a*, PP, and PIC—particularly along pathways to M1—highlighting reduced cross-shelf transfer and a stronger year-round influence of stratified tropical waters at that site.

During summer–autumn, weakened upwelling and intrusions of warm Mauritanian Current waters reduced surface productivity at both trap sites, yet deep organic matter export remained high—most prominently at CB but also at the

Formatted: English (UK)
Deleted: artament
Deleted: o
Formatted: English (UK)
Formatted: English (UK)
Formatted: English (UK)
Formatted: English (UK)
Formatted: English (UK)
Formatted: English (UK)
Deleted: fc
Formatted: Font: Italic
Formatted: Font: Italic
Deleted: Cape Blanc (CB)
Deleted: integrating lithogenic, organic, and coccolith species export …
Deleted: based
Deleted: ,
Formatted: Font: Italic
Formatted: English (UK)
Formatted: Font: Italic, English (UK)
Formatted: English (UK)
Formatted: English (UK)
Deleted: long
Formatted: Font: Italic, English (UK)
Formatted: English (UK)
Deleted: s
Deleted: and even

persistently oligotrophic M1. Across this period, elevated Saharan dust deposition coincided with enhanced particle fluxes. Multivariate statistical analyses show strong negative correlations between dust and all upper photic zone (UPZ) productivity indicators including Chl-*a*, the ratio of surface-dwelling species to lower photic zone taxa (UPZ/LPZ), and carbonate fluxes associated with the placolith-forming species *Emiliania huxleyi* and *Calcidiscus leptoporus*. In contrast, dust showed positive associations with warm, stratified conditions dominated by tropical, non-blooming LPZ species (*Florisphaera profunda* and *Gladiolithus flabellatus*), suggesting that mineral ballasting was the dominant seasonal dust effect. At CB, where summer cross-shelf transfer weakened, the persistence of high export regardless of low surface Chl-*a* suggests that lateral and subsurface supply of previously produced organic matter played a major role, with Saharan dust further enhancing its downward transfer through ballasting.

Nonetheless, several dust-associated export pulses also displayed increases in coccolith UPZ/LPZ ratios, suggesting episodic fertilisation responses by fast-blooming taxa superimposed on a broader ballasting-driven regime. Importantly, dust contributed under both windy, high-productivity late winter–spring conditions and during the stratified summer–autumn phase, sustaining downward particle flux even when local surface productivity was low. The weak relationship between AOD and measured dust flux reflects cloud-induced suppression of satellite AOD retrievals during wet deposition rather than reduced dust deposition.

Altogether, these results demonstrate a dual physical–atmospheric control on export in the central–southern CCS. Upwelling and cross-shelf transport fuel the winter–spring $CaCO_3$-rich export regime, whereas Saharan dust plays a particularly important role in maintaining organic-matter fluxes under summer–autumn stratification through ballasting, alongside episodic fertilisation responses. These findings contribute to refine the mechanistic understanding of coast-to-ocean and vertical export pathways and help constrain how dust–upwelling interactions will shape the biological carbon pump under future climate forcing.

1 Introduction

Despite covering only ~1 % of the ocean volume and < 3 % of the global ocean surface, eastern boundary upwelling systems (EBUS) account for ~5 % of global marine primary production (PP) and nearly 20 % of the global fish catch (Carr, 2002; Messié and Chavez, 2015), thus exerting a disproportionate influence on global nutrient and carbon cycling. This is particularly true for EBUS located adjacent to arid continental margins, where PP is co-driven by wind-driven upwelling of nutrient-rich subsurface waters and atmospheric transport and deposition of nutrient-bearing aerosols. Among them, the Canary Current System (CCS) stands out as the most prominent "dusty EBUS," positioned directly downwind of the Sahara Desert, the world's largest source of aeolian dust (Jickells et al., 2005; Yu et al., 2019).

Formatted: English (UK)
Formatted: Font: Italic, English (UK)
Formatted: English (UK)
Formatted: English (UK)
Formatted: English (UK)
Deleted: , and
Formatted: English (UK)
Formatted: English (UK)
Formatted: Font: Italic, English (UK)
Formatted: English (UK)
Formatted: Font: Italic, English (UK)
Formatted: English (UK)
Formatted: Font: Not Italic
Deleted: lower photic zone (
Deleted:)
Formatted: Font: (Default) Times New Roman, 10 pt, English (UK)
Deleted: taxa typical—
Deleted: as
Formatted: English (UK)
Deleted: under
Formatted: Font: Italic, English (UK)
Formatted: English (UK)
Deleted: mineral
Deleted: ¶
Deleted: with secondary
Formatted: English (UK)
Formatted: English (UK)

In the CCS, PP is sustained primarily by coastal upwelling, modulated by variability in trade-wind intensity, mesoscale eddy activity, and coastal and seafloor topography (e.g., capes) enhancing offshore export through the formation of upwelling filaments while locally acting as retention zones for biomass and nutrients (Arístegui et al., 2006, 2009; Santana-Falcón et al., 2020; Vazquez et al., 2022). At the same time, the region experiences strong atmosphere–ocean coupling driven by persistent Saharan dust transport, which delivers macronutrients and trace metals that complement upwelling inputs and further stimulate phytoplankton growth (Okin et al., 2011; Goudie and Middleton, 2001; Pabortsava et al., 2017; Guerreiro et al., 2023). Dust-derived iron has been reported to enhance N_2 fixation by diazotrophs (Prospero and Carlson, 1972; Jickells et al., 2005; Moore et al., 2009; Jickells et al., 2014; Brotas et al., 2023), increasing new nitrogen inputs and sustaining higher phytoplankton biomass and export production, thereby influencing the regional carbon cycle (e.g., Mahowald et al., 2014; Shelley et al., 2017; Brotas et al., 2023; Guerreiro et al., 2021; 2023; 2024). Additionally, mineral dust can also act as ballast, facilitating the export and long-term sequestration of particulate organic carbon (POC) in the deep ocean through the biological carbon pump (also known as "organic soft tissue" pump) (e.g., van der Jagt et al., 2018; Guerreiro et al., 2021; 2024). Export production, defined as the fraction of organic-carbon-rich material efficiently transported ("pumped") out of the upper ocean, thus represents a major pathway for atmospheric carbon removal and long-term climate regulation (Hutchins, 2011; Friedlingstein et al., 2022). Whether the higher productivity reported along the Mauritanian and Senegalese coasts compared to the northern sectors of the CCS (Arístegui et al., 2009) partly reflects the fertilizing influence of Saharan dust has yet to be investigated thoroughly.

Understanding these air-sea interactions and assessing the role of dust as a driver of the biological carbon pump are increasingly important considering ongoing climate change and the debate over long-term productivity trends in the CCS (e.g., Varela et al., 2015). In recent years, extreme warming events have intensified, with NOAA (2023) reporting Category 5 ("Beyond Extreme") marine heatwaves across the region (e.g., England et al., 2025). Such events, together with sustained ocean warming over the past decades, have been associated with pronounced shifts in phytoplankton community structure, including smaller cell sizes, reduced species diversity, deeper vertical distributions, and a rise in mixotrophic strategies (Dutkiewicz et al., 2013; Wilken et al., 2013; Balch et al., 2023; Zhan et al., 2024). These ecological changes are likely to propagate through the food web, diminishing fishery yields and weakening carbon sequestration, underscoring the urgent need for enhanced observation and predictive capacity (IPCC, 2023).

Unlike other major EBUS, the CCS has shown signs of weakening physical forcing, including reductions in trade wind intensity (1948–2017, Marrero-Betancort et al., 2020; 1980–2018, Polonsky and Serebrennikov, 2019) and upwelling strength (1967–2007; Barton et al., 2013; Gómez-Letona, 2017). Evidence for associated biological changes also remains inconclusive and highly dataset dependent. Arístegui et al. (2009) reported a general decline in satellite chlorophyll-*a* (Chl-*a*) between 1998 and 2007 from SeaWiFS data, though the short record and local variability limit trend robustness, particularly near the Mauritanian–Senegalese shelf. Using extended, multi-sensor records (1998–2017), Gómez-Letona et al. (2017) found minimal – and in some cases slightly positive – trends in Chl-*a* across the shelf, while trends in PP differed depending on the satellite

Deleted: —with
Deleted: , in particular,
Formatted: English (UK)
Formatted: English (UK)
Deleted: —
Deleted: —
Deleted: Whether higher productivity reported along the Mauritanian and Senegalese coasts compared to the northern sectors of the CCS (Arístegui et al., 2009) may partly reflect the fertilizing influence of Saharan dust, it has yet to be thoroughly investigated.
Formatted: English (UK)
Deleted: —
Formatted: English (UK)
Deleted: in
Formatted: Font: Italic, English (UK)
Formatted: English (UK)
Formatted: Font: Italic, English (UK)
Formatted: English (UK)
Deleted: —particularly near the Mauritanian–Senegalese shelf—
Deleted: -
Deleted: -
Deleted:
Formatted: English (UK)
Formatted: Font: Italic, English (UK)
Formatted: English (UK)

sensor data base and the satellite-based model employed. Siemer et al. (2021), applying the carbon-based production model (CbPm), reported regional warming north of 20°N accompanied by declines in Chl-*a* and PP since 2006. However, the CbPM is known to perform poorly in EBUS (Kahru et al., 2009; Hernández-Hernández et al., 2025), hence giving low confidence to those PP trends. In terms of export production, Fischer et al. (2019) documented a multi-year decline in organic carbon fluxes across all seasons from 2003 to 2016 at Cape Blanc coastal (eutrophic) upwelling site CBeu (NW Africa), which they interpreted as evidence of a long-term weakening of coastal upwelling off Cape Blanc. Overall, productivity patterns show high spatial and temporal variability but no consistent regional trend, underscoring the need for longer, multi-sensor datasets and *in situ* validation. Furthermore, while fertilizing nutrients and mineral ballast supplied by aeolian dust outbreaks may contribute to offset the projected weakening of the biological carbon pump (Pabortsava et al., 2017; van der Jagt et al., 2018; Guerreiro et al., 2021, 2023, 2024), disentangling the relative roles of dust and coastal upwelling remains challenging (e.g., Filipsson et al., 2011).

Sediment traps remain the dominant method for directly quantifying temporal variations in the bulk composition of vertical particle fluxes, including not only organic matter but also $CaCO_3$, biogenic silica, and lithogenic material, thereby providing essential ground-truthing data for assessing biogeochemical responses to climate forcing and to aeolian dust deposition in the ocean. With weekly to biweekly temporal resolution, they can capture both seasonal and episodic variability (e.g., dust events, upwelling pulses, eddy activity), helping to bridge the gap between surface production and deep-ocean sequestration.

Because coccolithophores enclose their cells in exoskeletons composed of calcite plates (coccoliths), they serve as valuable proxies for reconstructing recent and past open-ocean to coastal-neritic conditions (Baumann and Freitag, 2004; Guerreiro et al., 2015a,b), and are widely analysed in sediment-trap time series to resolve the seasonal to interannual dynamics of marine phytoplankton communities (e.g., Milliman, 1993; Sprengel et al., 2002; Baumann et al., 2005; Köbrich et al., 2015).

To address these gaps, we compared ~1 year of export production recorded by the Cape Blanc (CB) and M1 sediment traps, moored in the CCS downwind of major NW African dust sources, with satellite-inferred physical and biogeochemical data using both standard (Eulerian) and Lagrangian frameworks. This integrated approach identifies the source regions and trajectories of water masses that influence surface productivity and export fluxes, thereby linking biogeochemical variability with particle transport. Lagrangian particle tracking provides a dynamic, moving-frame perspective that enables the construction of biogeochemical budgets and reveals how nearshore production connects to offshore transport and deep-ocean export (Frischknecht et al., 2018; Hailegeorgis et al., 2021). Results are compared with satellite-derived records of upwelling indices, sea surface height (SSH) and aerosol optical depth (AOD) to disentangle the multiple environmental drivers shaping export production in the Canary Current EBUS under a warming North Atlantic.

Deleted: carbon-based CbPM model
Formatted: Font: Italic, English (UK)
Formatted: English (UK)
Deleted: the
Formatted: Font: Italic, English (UK)
Formatted: English (UK)
Deleted: mean of
Formatted: English (UK)
Deleted: carbon
Formatted: English (UK)
Formatted: English (UK)
Formatted: English (UK)
Formatted: English (UK)
Formatted: English (UK)
Deleted: in
Deleted: deep-sea sediment records used to
Deleted: open-ocean
Deleted: sediment traps
Deleted: c
Deleted: —
Deleted: —
Deleted: thickness

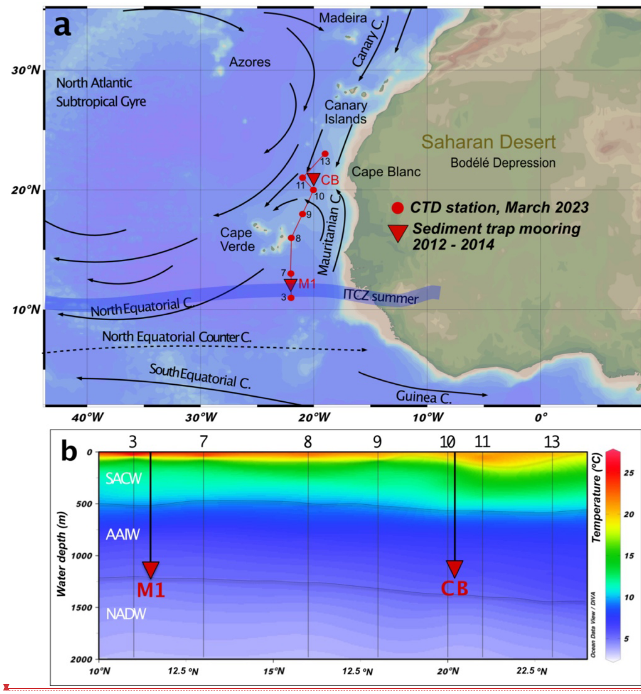

Figure 1: Location of the sediment trap mooring sites M1 and CB (triangles) and a schematic representation of (a) the main surface currents in the tropical and subtropical NE North Atlantic Ocean (adapted from Mann and Lazier, 2006) and of the ITCZ summer position (Basha et al., 2015), and (b) approximate vertical distribution of the main water masses present in the study area (SACW – South Atlantic Central Water; AAIW – Antarctic Intermediate Water; NADW – North Atlantic Deep Water) based on CTD profiles performed during 6–27 March 2023 on-board RV Pelagia (cruise PE514; Stuut et al., 2023).

2 Environmental settings

2.1 Water masses, large- and mesoscale surface ocean circulation

The environmental setting of the studied tropical NE Atlantic region has been previously presented in Guerreiro et al. (2019). Ocean conditions at sediment trap mooring sites CB and M1 are mostly influenced by South Atlantic Central Waters (SACW) at depths down to ~500 m (Temperature–T: 6.0–18°C, Salinity–S: 34.3–35.8) with substantial contributions of North Atlantic Central Waters (NACW) below 300 m. These waters originate from the North Atlantic subtropical gyre and are relatively nutrient-poor compared to SACW. The Antarctic Intermediate Water (AAIW), occupying depths below the thermocline to

Deleted:

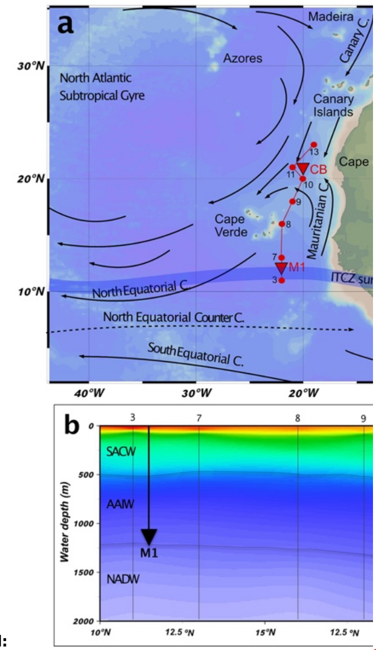

Formatted: English (UK)

Formatted: English (UK)

Formatted: English (UK)

Deleted: relatively nutrient-enriched

Deleted: originating from the North Atlantic subtropical gyre

Deleted: in its lower part (>

Deleted:)

Deleted: . The region hosts one of the world's major oxygen minimum zones (OMZs), with a shallow minimum (~80 m) driven by regional processes and a deeper one (~450 m) associated with gyre-scale ventilation (e.g., Karstensen et al., 2008; Fiedler et al., 2016; Brandt et al., 2015).

~1200 m, is distinguished by a pronounced salinity minimum and an accompanying oxygen maximum (Emery and Meincke, 1986; Reid, 1994; Stramma and England, 1999).

In the central–southern CCS, the mixed layer depth (MLD) is shaped both by large-scale, wind-driven shoaling of the thermocline across the tropical North Atlantic (Merle, 1980a,b; Katz, 1981; Guerreiro et al., 2019) and by dynamic eastern-boundary currents, fronts, and mesoscale features such as meanders, filaments, and eddies, that promote coastal–open ocean exchanges (Arístegui et al., 2009; Vázquez et al., 2021). The region also hosts one of the world's major oxygen minimum zones (OMZs), with a shallow minimum (~80) m driven by regional processes, and a deeper one (~450 m) associated with gyre-scale ventilation (e.g., Karstensen et al., 2008; Fiedler et al., 2016; Brandt et al., 2015).

Deleted: —

Deleted: —

Deleted: ¶

The Cape Blanc region (24–19° N), near CB, is shaped by the convergence of two major eastern boundary currents: the equatorward-flowing Canary Current and the poleward-flowing Mauritanian Current. Their interaction forms the persistent cyclonic Cape Verde Frontal System (CVFS; Barton, 1987; Zenk et al., 1991; Hernández-Guerra et al., 2005; Pastor et al., 2012), extending from Cape Blanc (~21° N) toward the Cape Verde Islands (~15° N). Here, the Canary Current detaches from the shelf to feed the westward North Equatorial Current (NEC), while the Mauritanian Current advects cooler, fresher SACW northward along the slope. The CVFS marks the convergence of these contrasting water masses, where tropical SACW meets the warmer, saltier NACW transported southward by the Canary Current (Pastor et al., 2012; Pelegrí et al., 2017, and references therein). Persistent coastal upwelling sustains intense offshore export of cold, nutrient-rich waters (Pastor et al., 2008; Alonso-González et al., 2009), largely driven by the long-lived Giant Cape Blanc Filament, which can extend up to 600 km offshore, transporting coastal waters to the open ocean (Van Camp et al., 1991; Gabric et al., 1993). High-chlorophyll waters are further entrained by eddies drifting southward along the Canary Current, which recirculate them coastward or advect them offshore through a corridor of cyclonic and anticyclonic eddies (Barton et al., 2004; Arístegui et al., 2009; Sangrá et al., 2009).

South of the CVFS, under more open-ocean conditions along the Mauritanian–Senegalese margin (19–10° N), the upper 100 m at M1 is dominated by warm, saline, nutrient-poor Tropical Surface Water (TSW; T ≈ 27 °C, S 36.7–37). Episodic intrusions of chlorophyll-enriched surface waters occur here, typically reaching their greatest offshore extent in spring (February–May) before rapidly declining in summer (Arístegui et al., 2009). Surface conditions are further influenced by offshore upwelling linked to the Guinea Dome, a quasi-stationary cyclonic feature modulated by seasonal shifts of the Intertropical Convergence Zone (ITCZ; Pelegrí et al., 2017). The dome, part of the large-scale near-surface circulation involving the westward-flowing NEC, the eastward-flowing North Equatorial Counter Current (NECC), and the North Equatorial Under Current (NEUC), strengthens and shifts onshore when the ITCZ moves south in winter–spring, and weakens and migrates offshore during its northward displacement in summer–autumn (Siedler et al., 1992; Pastor et al., 2013).

Deleted: and

2.2 Saharan dust deposition in the NE Atlantic Ocean

Atmospheric dust deposition over the ocean is highly variable and episodic, yet the NW African dust plume exhibits clear spatial and temporal gradients (Powell et al., 2015). These patterns are primarily driven by the seasonal migration of the ITCZ (Ben-Ami et al., 2012; Yu et al., 2019; van der Does et al., 2021), with the center of the main plume shifting from 10–20° N in summer to 0–10° N in winter (Adams et al., 2012). During boreal winter, the tropical NE Atlantic region closest to Saharan source regions receives the highest dust fluxes, mainly from Mauritania and Western Sahara, transported by low-altitude NE trade winds (Harmattan, 0–3 km) (Stuut et al., 2005; Skonieczny et al., 2013; Fomba et al., 2014; Fischer et al., 2016). In spring, frequent storms originating from Mauritania and Mali enhance deposition along the Senegalese margin (Goudie and Middleton, 2001; Skonieczny et al., 2013). During summer, the dust maximum shifts westward toward the Caribbean, carried by the elevated Saharan Air Layer (5–7 km) sourced mainly from the Sahel, particularly Mauritania and Mali (Goudie and Middleton, 2001; Stuut et al., 2005; Adams et al., 2012; Tsamalis et al., 2013; Prospero et al., 2014), whereas autumn generally corresponds to a period of minimum atmospheric loadings (Knippertz and Todd, 2012; Adams et al., 2012; Yu et al., 2019).

The impact of Saharan dust on the ocean depends on its concentration, deposition mode, and particle characteristics, which vary seasonally and along its westward transport pathway (Van der Does et al., 2016; 2020; Korte et al., 2017). Deposition is predominantly wet in summer and dry in winter, with dust becoming finer and less abundant farther from the African coast (Kok et al., 2014; Van der Does et al., 2016, 2020). Consequently, the dust reaching the Caribbean represents the fraction that survives wet removal during transport. These transatlantic patterns are reflected in surface-ocean chemistry, where elevated iron concentrations (~5–30° N) coincide with the Saharan dust plume (Baker et al., 2003; 2006; 2007; 2013; Bergquist and Boyle, 2006; Measures et al., 2008; Ussher et al., 2013; Shelley et al., 2017; Guerreiro et al., 2023). Short, but stronger pulse-like dust deposition events have been shown to fertilize the low-nutrient, low-chlorophyll (LNLC) waters of the tropical North Atlantic, enhancing productivity in the region (Guieu et al., 2014; Pabortsava et al., 2017; Guerreiro et al., 2017, 2023; Korte et al., 2020).

3 Methods

3.1 Sediment-trap sampling and particle flux time-series data

The *in situ* component of this study is based on published time-series data from two sediment-trap moorings that collected sinking particles at 1200 m depth during roughly the same one-year period in the open tropical NE Atlantic, off NW Africa (Fig. 1): Trap CB (21° N, 20° W), positioned in an open-ocean mesotrophic region (4160 m) influenced by upwelling off Cape Blanc (Mauritania), collected particles at variable intervals from 4 October 2012 to 21 February 2014; and Trap M1 (12° N, 23° W), located in a warmer, more stratified open-ocean setting (5000 m) near the southern limit of the CCS, sampled at 16-day intervals from 19 October 2012 to 7 November 2013. For details on the mooring setup, trap deployment and recovery, and sample processing, see Stuut et al. (2013), Korte et al. (2017), and Fisher et al. (2012, 2013, 2014). Temperature and pressure

Formatted: English (UK)
Deleted: —
Deleted: —
Deleted: shows
Formatted: Font: 10 pt, English (UK)
Formatted: Normal (Web), Justified, Don't add space between paragraphs of the same style, Line spacing: 1,5 lines
Formatted: Font: 10 pt, English (UK)
Formatted: Font: 10 pt, English (UK)
Deleted: and enhance productivity in
Formatted: Font: 10 pt, English (UK)
Formatted: Font: 10 pt, English (UK)
Formatted: Font: 10 pt, English (UK)
Deleted: ¶
Formatted: Font: 10 pt
Formatted: English (UK)

time-series from *in situ* sensors confirm that both traps remained vertical throughout deployment, and current velocities were consistently below the threshold that could compromise collection efficiency (Korte et al., 2017; Fisher et al., 2012, 2013, 2014). Flux data for $CaCO_3$ (proxy for calcifying plankton), $bSiO_2$ (proxy for diatoms), organic matter (proxy for carbon sequestration), and lithogenic material (proxy for Saharan dust) at traps M1 and CB are from Korte et al. (2017) and Guerreiro et al. (2019, 2021), respectively. Species-specific coccolith fluxes are from Guerreiro et al. (2019, 2021).

3.2 Lagrangian Analysis

To identify persistent source regions and dominant transport pathways of surface water masses influencing the sediment trap moorings, we used a Lagrangrian approach based on virtual particles advected in velocity fields generated by a General Circulation Model (GCM). We released tens of millions of virtual particles in the surface ocean off NW Africa and tracked those crossing the positions of traps CB and M1, within a 0.5° × 0.5° box around each site (smaller than their estimated catchment area; Guerreiro et al., 2019). Particles were stopped after crossing the box above the traps ("tails" removed) or after 60 days since their release, and any particles not crossing either box were removed from the analysis. The resulting water mass trajectories were matched with satellite-derived biogeochemical parameters, including Chl-*a*, PIC, and PP, to construct Lagrangian spatiotemporal time-series and biogeochemical budgets from the coast to the open ocean. We only include surface drifters and assume that the vertical flux of material was even and relatively fast (e.g., up to 40–150 m d^{-1} for algal aggregates, and 1–368 m d^{-1} for marine snow aggregates; Waniek et al., 2000 and refs. therein), thereby implying limited lateral displacement during export to the trap depth. This matching approach between virtual particles and satellite derived products is further described in Jönsson et al. (2009) and Jönsson and Salisbury (2016). The particle crossing times at each trap is defined as time zero (t = 0) and earlier positions have negative values down to t=-60 days. The setup allows us to track the evolution of surface ocean biogeochemical properties from the coast to each trap location. The resulting trajectories were then compared with seasonal particle fluxes captured at 1200 m by the traps to examine how *post-mortem* transformations of planktonic and dust-derived material influence particle export through the ocean water column.

3.3 Model Fields and Earth Observation Products

We used existing horizontal velocity fields from the Mercator Global Ocean Physics Reanalysis (GLORYS12V1), a data-assimilated, eddy-resolving (1/12° horizontal resolution, 50 vertical levels) global ocean reanalysis covering 1993–present (Lellouche et al 2018). Satellite-derived surface Chl-*a* and PP rates were used as proxies for phytoplankton biomass and productivity, respectively. The PP product, developed for the ESA PRIMUS project, was computed by a model of Morel (1991) with modifications described in Smyth et al. (2005). The model uses satellite-derived Chl-*a*, daily SST, Photosynthetic Available Radiance (PAR), day length, and either observed coloured dissolved organic material (CDOM) or an assumption of autochthonous CDOM. Concentrations of PIC, widely validated against *in situ* measurements from multiple locations (e.g., Balch et al., 2005), were used as a proxy for coccolithophore carbonate production at the surface (e.g., Hopkins et al., 2015).

Deleted: the
Deleted: fraction
Formatted: English (UK)
Deleted: —chlorophyll-a (
Deleted:)
Deleted: particulate inorganic carbon (
Deleted:)
Deleted: primary production rates (
Deleted:)—
Deleted: is
Formatted: Not Highlight
Formatted: Superscript
Deleted: s'
Deleted: s
Formatted: Font: Italic
Deleted: upper
Deleted: ¶
Formatted: English (UK)
Formatted: English (UK)
Formatted: Font: Italic
Deleted: surface

In addition to the biogeochemical parameters above, complementary Earth Observation data from multiple sources (listed in Table S1–Supplementary Material) were processed for the sediment-trap deployment period at CB and M1 to produce Fig. 2 and undertake the multivariate statistical analysis (section 3.4). Sea surface temperature (SST) was used as a proxy for thermal stratification (Signorini et al., 2015), mixed layer depth (MLD) indicated seasonal wind-driven water mixing, sea surface height (SSH) indicated variations in mesoscale eddy-activity, and temperature-derived Upwelling Index (UI) indicated the intensity of coastal upwelling along NW Africa. Combined with data of daily precipitation rates (DPP), these parameters were used to assess the seasonal influence of the ITCZ, with higher SST, higher rainfall, and shallower MLDs indicating greater ITCZ influence in the region (Oschlies and Garçon, 1998; Guerreiro et al., 2017, 2019). AOD 865 was employed as a measure of atmospheric aerosol load, used here as an indicator of dust originating from NW African deserts. Following the approach of Guerreiro et al. (2019, 2021), all the data were extracted within a 2° × 2° latitude–longitude box (~108 × 108 nautical miles; 1° ≈ 59 nm) around each trap site and averaged over each sediment-trapping interval for the study period (October 2012–October/November 2013 at M1 and extended to January 2014 at CB). This area was considered representative of the catchment region of a trap deployed at 1200 m depth, given the mean sinking speeds of marine phytoplankton and aggregates (e.g., Waniek et al., 2000).

3.4 Multivariate statistical analysis

To characterise the relationships between particle flux composition, coccolithophore taxa, and environmental conditions at CB and M1, we first computed a Pearson correlation coefficient matrix using a dataset of 43 samples and 19 variables, with p-values corrected for multiple comparisons using the Bonferroni correction. The variables included the percentage contributions of major coccolith taxa (fast-blooming placolith-bearing *Emiliania huxleyi*, *Gephyrocapsa* spp., *Calcidiscus leptoporus* and *Umbilicosphaera* spp.; tropical surface-dwelling *Rhabdosphaera* spp. and *Umbellosphaera* spp., tropical deep-dwelling *Florisphaera profunda* and *Gladiolithus flabellatus*; and tropical-mesotrophic *Helicosphaera* spp.) and the percentages of $CaCO_3$, $bSiO_2$, organic matter, and lithogenic material (i.e., dust) together with satellite-derived parameters (Chl-*a*, PIC, SST, MLD, AOD, and DPP). The UPZ/LPZ ratio—derived from UPZ (*E. huxleyi* + *Gephyrocapsa* spp.) vs. LPZ (*F. profunda* + *G. flabellatus*) taxa—was included as a proxy for thermocline/nutricline dynamics (Guerreiro et al., 2019). Satellite-inferred PP was excluded due to its strong dependence on Chl-*a* and additional model uncertainties.

A Principal Component Analysis (PCA, correlation mode; PAST 4.0) using the same dataset was then applied to reduce dimensionality and identify the dominant modes of variability across both moorings. PCA scores were plotted through time to evaluate the seasonal evolution of export regimes at CB and M1. Both the Pearson correlations and the PCA were performed on percentage-based (compositional) data rather than absolute fluxes to minimize covariance driven by variations in total mass flux, an inherent property of sediment-trap records, thereby reducing artefactual correlations associated with the co-sinking of particles from different origins. Using relative contributions emphasises ecological and mechanistic relationships among

Formatted: English (UK)
Deleted: .
Formatted: Font: Not Italic
Formatted: Font: Not Italic
Deleted: (lithogenic particles),
Formatted: Font: Italic
Deleted: daily precipitation
Formatted: Font: Italic
Formatted: Font: Not Italic
Formatted: Font: Not Italic
Deleted: —
Deleted: —
Deleted: caused by
Deleted: with

sinking coccolith species, particle flux components, and environmental drivers, offering a clearer assessment of potential ballasting effects and environmental controls on export production.

4 Results

4.1 Environmental conditions and particle export fluxes at M1 and CB

Formatted: English (UK)

As reported from previous studies, site M1 exhibited generally more stable MLD seasonal dynamics compared to CB, primarily influenced by latitudinal shifts of the ITCZ (Korte et al., 2017; Guerreiro et al., 2019, 2021). Conditions transitioned from slightly deeper mixed layers (~35 m) and cooler SST (down to 24 °C) during the windy, dry winter–spring months, to shallower mixed layers (as little as ~11 m) and warmer SST (up to 29 °C) during the calmer, wetter summer–autumn period. Although broadly similar seasonally, site CB exhibited a more pronounced MLD cycle, driven primarily by fluctuations in the intensity of year-round upwelling off Cape Blanc and, to a lesser extent, by ITCZ migration. This was reflected in the broader MLD range (20–73 m), generally cooler SST (19–26 °C), and much lower precipitation rates compared to M1 (Figs. 2a,b).

Deleted: MLDs

Deleted: MLDs

Although AOD displayed comparable ranges at both trap sites, its temporal evolution showed pronounced month-to-month variability, particularly at CB, highlighting the highly dynamic nature of Saharan dust outflow in the region. At M1, moderately high AOD persisted through autumn–winter (November 2012–February 2013), transitioned to a more variable pattern in spring with a moderate peak in April and a maximum in June, and then declined during summer. In contrast, CB exhibited much lower AOD during autumn–winter 2012, followed by a sharp increase in February and a major peak in June–July. After this period, AOD returned to moderate summer values before decreasing to low levels in the subsequent autumn–winter (Fig. 2a). Dust fluxes at 1200 m also showed stronger variability at CB than at M1, with both sites experiencing abrupt, high-magnitude deposition events that did not consistently coincide with AOD maxima. Episodic dust pulses at CB (up to 57–114 mg m^{-2} d^{-1}) occurred in February–March, mid-May, and from mid-July until October 2013, whereas M1 recorded somewhat lower but steadier peaks (61–71 mg m^{-2} d^{-1}) in March, and from mid-June until late September. Despite CB exhibiting more intense episodic events, the more regular seasonal export regime at M1 resulted in a higher mean annual dust flux (48 mg m^{-2} d^{-1}) compared to CB (38 mg m^{-2} d^{-1}), consistent with the higher mean AOD at M1 (Fig. 2e; Table S2, Supplementary Material). The strongest mismatches between AOD and dust flux occurred during autumn–winter at M1, where elevated AOD from December 2012 to January 2013 coincided with lower dust flux, followed by a major flux peak in February–March during an

Deleted: —

Deleted: —

Deleted: —

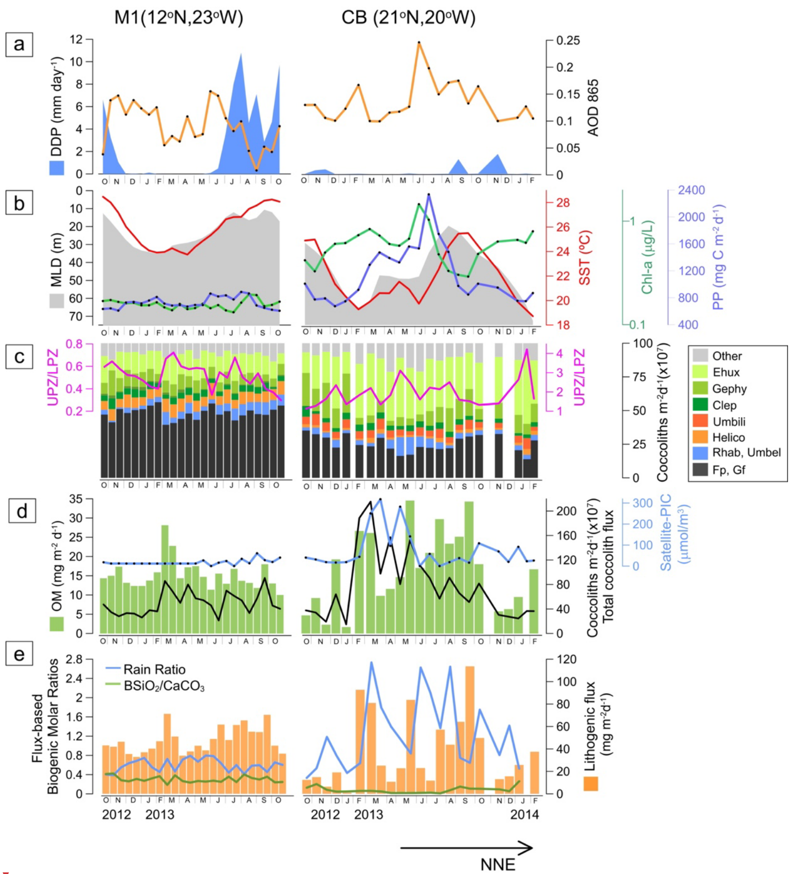

Figure 2: Spatiotemporal variation of (a) daily precipitation rates (light blue) and aerosol optical depth (AOD, orange line), (b) mixed layer depth (MLD, dark blue), sea surface temperature (SST, red line), surface Chl-*a* concentrations (green line), and primary production (PP, purple line), (c) relative abundances of the main coccolith sinking taxa (vertical bars), and coccolith-UPZ/LPZ ratio (purple line; used as a proxy for nutricline depth dynamics; Guerreiro et al. 2017, 2019), (d) fluxes of organic matter (OM, green bars), satellite-PIC concentrations (blue line), and total coccolith fluxes (black line), and (e) lithogenic flux (orange bars), rain ratio ($CaCO_3$/POC, blue line), and the molar ratio between fluxes of biogenic silica and $CaCO_3$ ($bSiO_2$/$CaCO_3$, green line) used as a proxy for the ratio of silicifying to calcifying plankton (see Cermeño et al. 2008). The lithogenic flux (i.e., residual fraction) results from subtracting the weights of biogenic constituents (i.e., $CaCO_3$, organic matter and $bSiO_2$) from the total mass flux, and has been used as a proxy for dust deposition in the Atlantic Ocean (Jickells et al., 1998), including our study area (e.g., Fischer et al. 2016; Guerreiro et al. 2017, 2021; Korte et al. 2017). Data sources: Korte et al. (2017), Guerreiro et al. (2019, 2021).

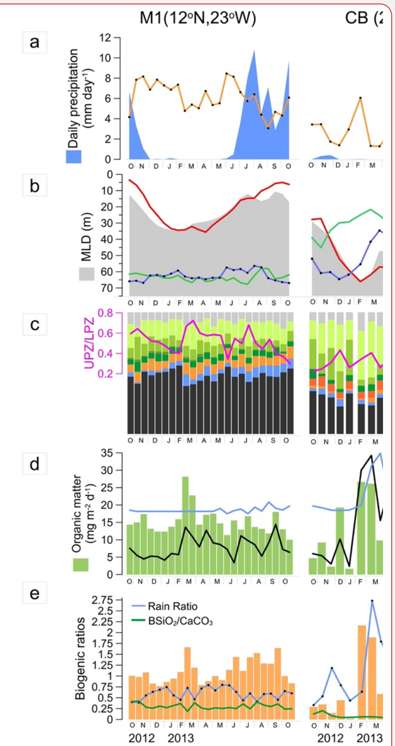

Deleted:

Deleted: thickness

Deleted: surface

Deleted: “

Deleted: ”

Deleted: ve

Deleted: 1).

AOD minimum; and during summer–autumn at CB, where the AOD maximum in June–July coincided with a dust flux minimum, while the dust peak in late September aligned with a drop in AOD (Fig. 2a,e).

Seasonal contrasts in atmospheric (wind, precipitation, dust) and upper-ocean (MLD, SST) conditions between the two sites (Figs. 2a,b) were reflected in pronounced differences in surface productivity and in both the magnitude and composition of their export fluxes (Figs. 2b–d). The new satellite-driven PP data used in this study are consistent with previously reported patterns, co-increasing with surface Chl-*a* and PIC concentrations, all of which higher at M1 than at CB. These patterns were accompanied by generally higher, more seasonal, and carbonate-rich fluxes at CB compared to M1, including coccoliths, particularly from late winter to spring (Figs. 2b–d). At CB, coccolith assemblages were dominated by placolith-bearing taxa, including opportunistic (r-selected) UPZ species (*E. huxleyi*, *Gephyrocapsa* spp., *C. leptoporus*), whereas at M1, higher proportions of coccoliths were produced by species typical of warmer, stratified conditions, such as deep-dwelling LPZ taxa (*F. profunda*, *G. flabellatus*), K-selected surface-dwellers (*Umbellosphaera*, *Rhabdosphaera* spp.), and large miscellaneous forms (*Helicosphaera* spp.) (Figs. 2c,d; Table S2 – Supplementary Material).

Despite markedly higher surface PP and Chl-*a* concentrations over CB, the higher carbonate fluxes and rain ratios ($CaCO_3$/POC), together with lower $bSiO_2$ fluxes recorded at 1200 m, suggest that the biological carbon pump did not operate more efficiently there than at the warmer M1 site. Although CB showed slightly higher episodic peaks in organic matter flux (27–35 mg m^{-2} d^{-1} in late January, mid-May, mid-July, and mid-September) than M1 (23–28 mg m^{-2} d^{-1} from late February to mid-March), the steadier seasonal export regime at M1 resulted in similar mean annual POC fluxes at both sites (15 and 17 mg m^{-2} d^{-1} at M1 and CB, respectively) (Figs. 2d,e; Table S2 – Supplementary Material).

4.2 Multivariate statistical analysis

Pairwise Pearson correlations revealed significant structure among coccolithophore taxa, particle fluxes, and environmental variables (Table 1). *E. huxleyi*, *C. leptoporus*, and *Umbilicosphaera* spp. were strongly positively correlated ($r \approx 0.72$–0.91), indicating coherent productivity patterns among fast-blooming placolith-bearing species typical of the UPZ. Deep-dwelling *F. profunda* and *G. flabellatus* showed no significant correlations with this group, reflecting their distinct ecological niches, although they were moderately positively correlated with *Umbilicosphaera* spp. ($r \approx 0.49$) and *Gephyrocapsa* spp. ($r \approx 0.42$). *Rhabdosphaera* and *Umbellosphaera* spp. displayed non-significant weak positive correlations with both placolith-bearing and deep-dwelling taxa ($r \approx 0.29$–0.43), consistent with their affinity for tropical, stratified conditions while typically thriving in the upper photic zone. *Helicosphaera* spp. correlated strongly and significantly with deep-dwellers ($r \approx 0.87$), in line with its higher coccolith fluxes at the more tropical site M1. *Gephyrocapsa* spp. had no significant correlations with any other taxa, although they displayed positive correlations with *Umbilicosphaera* spp., *Helicosphaera* spp. and deep-dwelling taxa ($r \approx$ 0.42–0.46), suggesting a relatively mesotrophic preference during the studied period.

Deleted: from
Deleted: SSW to
Formatted: Font: Italic
Deleted: NNE,
Deleted: —including coccoliths—
Deleted: with
Deleted: elevated values
Deleted: d
Deleted: with comparable
Deleted: c
Deleted: y
Deleted: yielded
Deleted: carbon
Formatted: English (UK)
Deleted: surface-dwelling
Deleted: associations
Deleted: except for a moderate correlation with *Umbilicosphaera* spp. ($r \approx 0.49$)
Deleted: .
Deleted:
Deleted: -to-moderate
Deleted: ; and
Deleted: ted significantly only
Deleted:
Formatted: Font: Italic

The UPZ/LPZ ratio showed positive significant correlations with Chl-*a*, MLD and $CaCO_3$ (r ≈ 0.55–0.70) and weakly positive non-significant correlations with *E. huxleyi*, *C. leptoporus*, and satellite PIC (r ≈ 0.35–0.43). In contrast, it displayed strong negative significant correlations with deep-dwelling taxa, *Helicosphaera* spp., SST, $bSiO_2$, and lithogenic flux (r ≈ 0.73–0.76). Coccolith-$CaCO_3$ fluxes correlated strongly and significantly with fast-blooming placolith-bearing taxa (r ≈ 0.70–0.83) and showed positive but non-significant correlations with *Rhabdosphaera* and *Umbellosphaera* spp. (r ≈ 0.49) and satellite-PIC (r ≈ 0.41), while showing a non-significant negative correlation with OM (r ≈–0.41). Satellite-derived PIC only showed significant positive correlations with *E. huxleyi* (r ≈ 0.53) and non-significant positive correlations with *C. leptoporus* (r ≈ 0.49), UPZ/LPZ, coccolith-$CaCO_3$, $CaCO_3$, Chl-*a*, and MLD (r ≈ 0.36–0.43). Lithogenic flux was positively and significantly correlated with *Helicosphaera* spp., SST, DPP, and $bSiO_2$ (r ≈ 0.52–0.70) and displayed a positive but non-significant correlation with deep-dewlling taxa (r ≈ 0.49). In contrast, it showed strong and significant negative correlations with high surface productivity indicators, including UPZ/LPZ, Chl-*a*, MLD and $CaCO_3$ (r ≈ 0.54–0.90) (Table 1).

Overall, UPZ/LPZ, Chl-*a*, MLD, and carbonate-associated variables covaried with surface, fast-blooming placolith-bearing taxa, whereas SST, $bSiO_2$, DPP, AOD, and lithogenic flux covaried with tropical taxa indicative of warmer, more stratified, dust-influenced conditions (Table 1).

Table 1. Pearson correlation coefficient matrix showing the relationships among the variables included in the data matrix used in the PCA. Correlation coefficients are shown as Pearson's *r* values, with statistically significant correlations ($p < 0.05$) after Bonferroni correction for multiple comparisons highlighted in bold and grey (light grey for negative correlations; dark greyfor positive correlations). Non-significant correlations with |*r*| ≥ 0.36 are not highlighted and shown in black, whereas weaker correlations are shown in grey. The full names of the coccolithophore taxa and environmental parameters are indicated in Table 2.

	Ehux	Gephy	Clep	Helico	Rhab & Umbell	Fp & Gflab	Umbilli	UPZ/LPZ	Coccolith-$CaCO_3$	Chl-*a*	SST	AOD	DPP	MLD	$CaCO_3$	$bSiO_2$	OM	Lithogenic	PIC
Ehux	1	0,16	**0,91**	-0,09	0,43	0,13	**0,72**	0,37	**0,83**	0,44	-0,47	-0,17	-0,20	0,41	0,51	-0,45	-0,40	-0,35	**0,53**
Gephy	0,16	1	0,27	0,42	-0,04	0,42	0,46	-0,30	0,30	-0,31	0,30	0,29	0,06	-0,39	-0,04	0,29	-0,15	0,10	-0,08
Clep	**0,91**	0,27	1	-0,15	0,30	0,04	**0,72**	0,35	**0,81**	**0,54**	**-0,51**	-0,12	-0,26	0,44	0,50	-0,52	-0,32	-0,35	0,49
Helico	-0,09	0,42	-0,15	1	0,24	**0,87**	0,29	**-0,73**	0,16	**-0,67**	**0,60**	0,39	0,39	**-0,59**	-0,49	**0,72**	-0,13	**0,52**	-0,22
Rhab & Umbell	0,43	-0,04	0,30	0,24	1	0,34	0,29	-0,06	0,49	0,00	0,03	0,02	0,26	-0,12	0,08	-0,21	-0,20	0,07	0,25
Fp & Gflab	0,13	0,42	0,04	**0,87**	0,34	1	0,49	**-0,76**	0,25	**-0,60**	**0,57**	0,46	0,36	**-0,55**	-0,40	**0,64**	-0,23	0,49	-0,17
Umbilli	**0,72**	0,46	**0,72**	0,29	0,29	0,49	1	-0,08	**0,70**	0,13	-0,10	0,16	-0,02	0,06	0,23	-0,03	-0,37	-0,10	0,31
UPZ/LPZ	0,37	-0,30	0,35	**-0,73**	-0,06	**-0,76**	-0,08	1	0,13	**0,70**	**-0,75**	-0,48	-0,39	**0,70**	**0,55**	**-0,76**	-0,12	**-0,62**	0,43
Coccolith-$CaCO_3$	**0,83**	0,30	**0,81**	0,16	0,49	0,25	**0,70**	0,13	1	0,25	-0,23	-0,08	-0,04	0,11	0,34	-0,31	-0,41	-0,15	0,41
Chl-*a*	0,44	-0,31	**0,54**	**-0,67**	0,00	**-0,60**	0,13	**0,70**	0,25	1	**-0,81**	-0,19	-0,36	**0,70**	**0,69**	**-0,81**	-0,18	**-0,64**	0,36
SST	-0,47	0,30	**-0,51**	**0,60**	0,03	**0,57**	-0,10	**-0,75**	-0,23	**-0,81**	1	0,34	**0,62**	**-0,90**	**-0,66**	**0,69**	0,04	**0,70**	-0,38
AOD	-0,17	0,29	-0,12	0,39	0,02	0,46	0,16	-0,48	-0,08	-0,19	0,34	1	0,07	-0,45	-0,16	0,31	-0,13	0,23	-0,53
DPP	-0,20	0,06	-0,26	0,39	0,26	0,36	-0,02	-0,39	-0,04	-0,36	**0,62**	0,07	1	**-0,58**	-0,46	0,24	-0,06	**0,56**	-0,12
MLD	0,41	-0,39	0,44	**-0,59**	-0,12	**-0,55**	0,06	**0,70**	0,11	**0,70**	**-0,90**	-0,45	**-0,58**	1	0,49	**-0,58**	0,11	**-0,54**	0,40
$CaCO_3$	0,51	-0,04	0,50	-0,49	0,08	-0,40	0,23	**0,55**	0,34	**0,69**	**-0,66**	-0,16	-0,46	0,49	1	**-0,64**	-0,30	**-0,90**	0,42
$bSiO_2$	-0,45	0,29	-0,52	**0,72**	-0,21	**0,64**	-0,03	**-0,76**	-0,31	**-0,81**	**0,69**	0,31	0,24	**-0,58**	**-0,64**	1	0,07	**0,54**	-0,46
OM	-0,40	-0,15	-0,32	-0,13	-0,20	-0,23	-0,37	-0,12	-0,41	-0,18	0,04	-0,13	-0,06	0,11	-0,30	0,07	1	0,14	-0,33
Lithogenic	-0,35	0,10	-0,35	**0,52**	0,07	0,49	-0,10	**-0,62**	-0,15	**-0,64**	**0,70**	0,23	**0,56**	**-0,54**	**-0,90**	**0,54**	0,14	1	-0,35
PIC	**0,53**	-0,08	0,49	-0,22	0,25	-0,17	0,31	0,43	0,41	0,36	-0,38	-0,53	-0,12	0,40	0,42	-0,46	-0,33	-0,35	1

Moved down [1]: *E. huxleyi*, *C. leptoporus*,

Deleted: ,

Formatted: Font: Italic

Moved (insertion) [1]

Deleted: ,

Formatted: Font: Italic

Deleted: correlated positively with the placolith group,

Deleted: .

Formatted: Font: Italic

Deleted: tropical taxa,

Formatted: Font: Italic

Deleted: ,

Formatted: Font: Italic

Formatted: Font: Italic

Deleted: ¶ ... [1]

Formatted: Font: 9 pt, Bold

Deleted: ¶

Formatted: Font: Times, 9 pt, Bold

Deleted:

Pearson Correlation (p<0.05)	Ehux	Gephy	Clep	Helico	Rhab & Umbell
Ehux		0,16	**0,91**	-0,09	0,43
Gephy	0,16		0,27	0,42	-0,04
Clep	**0,91**	0,27		-0,15	0,30
Helico	-0,09	0,42	-0,15		0,24
Rhab & Umbell	0,43	-0,04	0,30	0,24	
Fp & Gflab	0,13	0,42	0,04	**0,87**	0,34
Umbilli	**0,72**	**0,46**	**0,72**	0,29	0,29
UPZ/LPZ	0,37	-0,30	0,35	**-0,73**	-0,06
Coccolith-$CaCO_3$	**0,83**	0,30	**0,81**	0,16	**0,49**
Chl-a	0,44	-0,31	**0,54**	**-0,67**	0,00
SST	**-0,47**	0,30	**-0,51**	**0,60**	0,03
AOD	-0,17	0,29	-0,12	0,39	0,02
DPP	-0,20	0,06	-0,26	0,39	0,26
MLD	0,41	-0,39	0,44	**-0,59**	-0,12
$CaCO_3$	**0,51**	-0,04	**0,50**	**-0,49**	0,08
$bSiO_2$	**-0,45**	0,29	**-0,52**	**0,72**	-0,21
OM	-0,40	-0,15	-0,32	-0,13	-0,20
Lithogenic	-0,35	0,10	-0,35	**0,52**	0,07
PIC	**0,53**	-0,08	0,49	-0,22	0,25

¶

To synthesize these multiple interrelationships and visualize the main sources of variance across space and time, a PCA was performed. The first two principal components (PCs) together explained 62.3% of the total variance, highlighting the main differences between the two sediment-trap sites (Fig. 3, Table 2). PC1 (39.8%) reflected a contrast between two groups of variables that are very much in line with the significant correlations obtained from the Pearson correlation analysis. Positive loadings included UPZ/LPZ ratio, Chl-*a*, MLD, and $CaCO_3$ fluxes, with weaker contributions from *E. huxleyi*, *C. leptoporus* abundances and satellite-driven PIC; and negative loadings wer dominated by *Helicosphaera* spp., SST, $bSiO_2$, and lithogenic flux, with smaller contributions from *F. profunda*, *G. flabellatus*, AOD and DPP. At CB, PC1 scores were mostly positive during most of the sampling period, and exhibited a pronounced seasonal cycle, with strong positive values from late winter and to early summer 2013, and then again in late winter 2014. At M1, scores followed a broadly similar temporal pattern but remained consistently negative and more stable (Fig. 3, Table 2).

Deleted: Principal Component Analysis (

Deleted:)

Deleted: clusters

Deleted: dust

Deleted: daily precipitation

PC2 (22.5%) is defined by positive loadings from coccolith-$CaCO_3$ and several taxa, including both fast-blooming (*Umbilicosphaera* spp., *E. huxleyi*, *C. leptoporus*) and tropical (*F. profunda*, *G. flabellatus*, *Helicosphaera*, *Rhabdosphaera* spp. and *Umbellosphaera* spp.); and negative loadings associated with organic matter. At M1, PC2 scores were mostly positive but remained close to zero throughout the record, whereas CB showed greater variability, with negative scores prevailing in autumn–winter and a distinct positive pulse from late January to early March 2013 (Fig. 3, Table 2).

Deleted: –

Deleted: from

Deleted: ¶

Table 2: Principal components (PCs), eigenvalues, and percentages of explained variance were extracted from the data matrix covering the sediment trap sampling period from October 2012 to November 2013 at mooring M1, and until February 2014 at mooring CB (PCA in correlation mode, performed in PAST 4; loadings ≥ 0.3 and ≤ -0.3 marked in bold, highlighted in dark grey and light grey, respectively). Data sources: Korte et al. (2017); Guerreiro et al. (2019, 2021).

Deleted: blue and black

Variables	PC 1	PC 2
Ehux - *Emiliania huxleyi*	0,2	**0,3**
Gephy - *Gephyrocapsa* spp.	-0,1	**0,3**
Clep - *Calcidiscus leptoporus*	0,2	**0,3**
Helico - *Helicosphaera* spp.	**-0,3**	**0,3**
Rhabdo&Umbell - *Rhabdosphaera* spp. & *Umbellosphaera* spp.	0	**0,3**
Fp&Gf - *Florisphaera profunda* & *Gladiolithus flabellatus*	-0,2	**0,3**
Umbilli - *Umbilicosphaera spp.*	0,1	**0,4**
Coccolith-UPZ/LPZ	**0,3**	-0,1
Coccolith-$CaCO_3$ - Coccolithophore calcium carbonate	0,1	**0,4**
$CaCO_3$ - Total calcium carbonate	**0,3**	0,1
$bSiO_2$ - Biogenic silica	**-0,3**	0
Organic Matter	-0,1	**-0,3**
Litho - Lithogenic flux	**-0,3**	0
PIC - Particulate Inorganic Carbon	0,2	0,1
Chl-*a* Chlorophyll-*a*	**0,3**	0
SST - Sea Surface Temperature	**-0,3**	0,1
AOD - Aerosol Optical Depth	-0,2	0,1
DPP - Daily Precipitation rates	-0,2	0,1
MLD - Mixed Layer Depth	**0,3**	-0,1
Eigenvalues	7,56	4,27
Explain. Var (%)	39,8	22,5

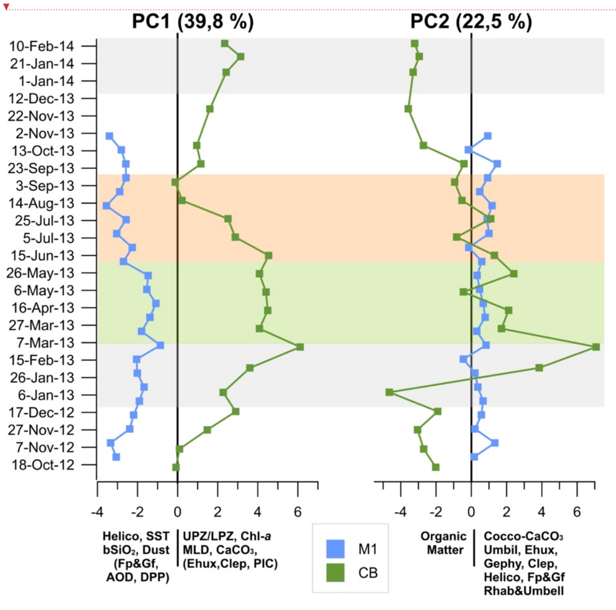

Figure 3: Spatiotemporal variation in the scores obtained from PCA. For taxonomical references, see Table 2. Horizontal bars represent the Northern Hemisphere seasons: grey–winter, green–spring, orange–summer, white–autumn.

4.3 Lagrangian analysis of surface water mass trajectories

The Lagrangian analysis tracking particles from the near coast to the traps show notable differences in the origin and persistence of how coastal waters are influencing the traps. CB was consistently affected by coastal masses advected from the E–NE and/or SE throughout the study period, whereas at M1 such influences occurred only seasonally and were comparably weaker (Fig. 4). At CB, surface conditions were influenced by NE-derived waters year-round but more strongly from boreal spring to summer (March–July 2013 and March–May 2024) while, during the intervening months, SE-derived waters also influenced circulation in the region, particularly from late summer to autumn (December 2012 and August–October 2013, and more weakly in November–December 2013) (Fig. 4). At M1, NE-derived waters exerted the strongest influence in spring and early summer (March–June 2013 and March–May 2014). Before spring, the site was only intermittently affected by waters arriving from the ENE and from the ESE (November–December 2012 and December 2012–February 2014). From summer to

Deleted: Variables ... [2]

Deleted: ¶

Formatted: English (UK)

Deleted: notable

Deleted: markedly

Deleted: were

Deleted: persistent

Deleted: early

Deleted: 3

Deleted: 7

Deleted: and reappeared, though less strongly, in boreal autumn (13 October–10 November 2013). D

Deleted: 18

Deleted: 13

Deleted: ¶ ¶

Deleted: ,

Deleted: though these appeared to originate offshore near Cape Verde (~14° N, 22° W) rather than from the Mauritanian coast.

Deleted: late September 2012

Deleted: early March

Deleted: 3

autumn (July–December 2013), M1 remained largely isolated from wind-driven surface mixing, after which waters advected from NE resumed their influence until February 2014 (Fig. 4).

4.4 Lagrangian backtracking trajectories of biogeochemical parameters

Lagrangian tracking allowed us to follow the evolution of Chl-*a*, PIC, and PP in surface waters from the upwelling region to the traps in time increments averaged at the sediment-trap sampling resolution (~two weeks) before, during, and after the sediment trap deployment (October 2012–May 2014; Figs. 5–7; July 2012–May 2014; Fig. 8). The resulting figures reveal spatiotemporal patterns consistent with the seasonal surface-water trajectories described in Section 4.3.

At CB, Chl-*a*- and PP-enriched waters originating from both the NE and SE between October 2012 and January 2013 progressively shifted toward predominantly NE sources in late winter–spring, when offshore export was most efficient. In contrast, the summer–early autumn period (June–September 2013) showed the lowest Chl-*a* and PP, with productivity recovering from October 2013 to May 2014, again increasingly linked to NE-sourced waters towards spring. At M1, productive coastal influence was also linked to NE-derived water masses, peaking in spring 2013 (from March to May) and briefly reappearing in December 2013, becoming increasingly associated with NE-sourced waters towards April.

While PIC followed similar spatiotemporal trends as Chl-*a* and PP, overall concentrations remained low, suggesting limited carbonate production and/or weaker offshore transport. At CB, surface waters were particularly PIC-poor from June to September 2013, whereas M1 remained largely unaffected by PIC-enriched waters year-round (Fig. 7).

Deleted: 7

Deleted: 8

Formatted: English (UK)

Deleted: of

Deleted: late September

Deleted: mid-February

Deleted: a

Deleted: c

Deleted: anuary

Deleted: December

Deleted: s

Deleted: 6a–c

Deleted:

Deleted:

Deleted: February

Deleted: especially

Deleted: late

Deleted: –January 2014, but remained weak throughout the rest of the record.…

Deleted: to

Deleted: PIC-rich

Deleted: scarce

Deleted: late May

Deleted: 5c

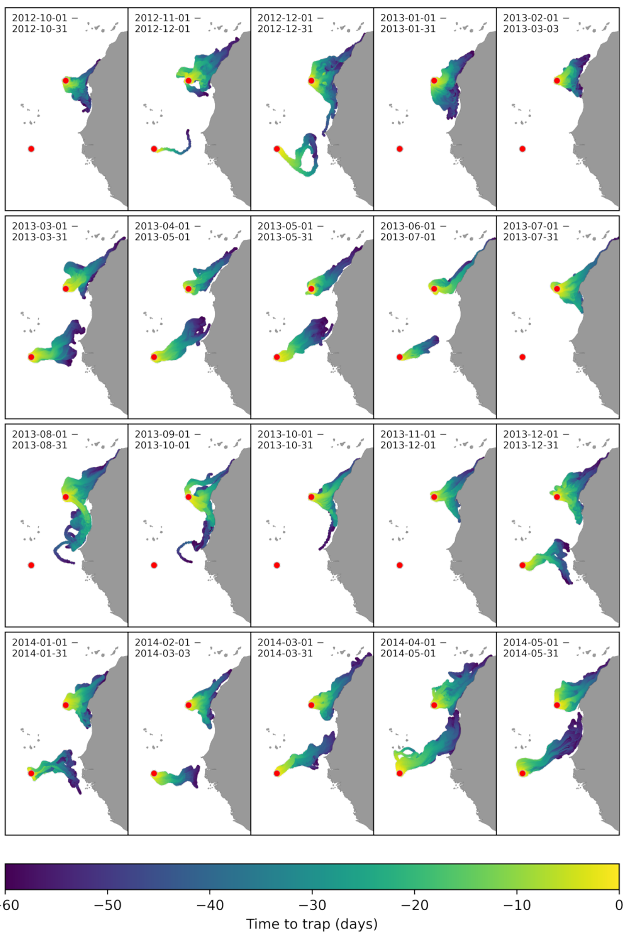

Deleted:

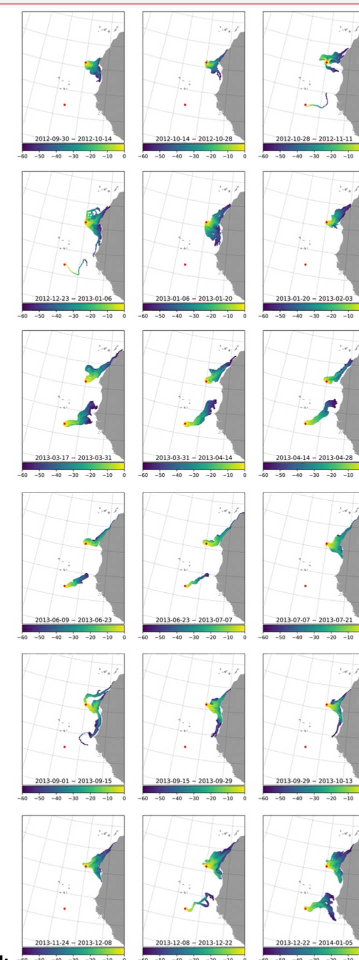

Figure 4: Lagrangian trajectories of surface water masses tracked from virtual particles seeded from the NW African coast and subsequently advected offshore. Only the trajectories crossing the location of at least one of the trap moorings are included (red dots indicate the location of mooring sites CB and M1). Time intervals coincide with those of the sediment traps for the studied year (from October 2012 to February 2014).

Lagrangian backtracking trajectories (Fig. 8) confirm these trends, showing coastal origins of generally higher Chl-*a*, PIC, and PP up to > 50 days prior to trap arrival, generally declining offshore toward the trap sites (schematic representation shown in Fig. 8). The decline was steepest for PIC, particularly near M1, and overall concentrations of Chl-*a*, PIC, and PP were consistently higher along pathways to CB.

At CB, enhanced surface Chl-a occurred during two main periods: October 2012–May 2013 and October 2013–February 2014. Within these intervals, December 2012, late January to mid-March 2013, and February 2014 were marked by a good correspondence between high surface biomass and strong organic matter export. However, from mid-May to October 2013, the occurrence of high export fluxes despite low surface Chl-*a* suggests a decoupling between surface productivity and export. The UPZ/LPZ ratio aligned well with both Chl-*a* and export from December 2012–March 2013, and again with export in summer and surface Chl-*a* in late 2013–early 2014 (Fig. 8).

At M1, surface productivity was consistently lower than at CB, both near the coast and at the trap, with satellite data showing long periods without detectable Chl-a in the Lagrangian backtracking trajectories (Fig. 8). Slightly more elevated surface Chl-*a* occurred in December 2012 and March–May 2013, followed by low values until November 2013, reflecting a shorter productive season. Chl-*a* declined sharply up to 30 days before reaching M1, suggesting early depletion of coastal biomass. A brief coupling between Chl-*a*, enhanced export, and UPZ/LPZ ratios occurred in March 2013. Following this pulse, export fluxes returned to pre-March levels despite no Chl-*a* observed at the surface, while the UPZ/LPZ ratio showed a more variable pattern, with increases in March, May and late July 2013. Interannual variability was higher near M1, with stronger surface Chl-*a* signals closer to the trap in January and February 2014 than in 2013.

Satellite-derived PP patterns paralleled Chl-*a* at both traps, with the highest rates from late winter to spring 2013 and minima in summer, though the coastal-to-offshore gradient was less steep (Fig. 8). PIC showed similar coast–CB gradients but was nearly absent near M1, dropping to zero much closer to the coast. At CB, surface PIC displayed a clear seasonal cycle, closely tracking coccolith export and UPZ/LPZ ratios from late autumn through May 2013, while PIC was only slightly over M1 during in December 2012 and April 2013 (Fig. 8).

Deleted: s
Deleted: 6a–d
Deleted: elevated
Formatted: Not Highlight
Deleted: 6
Deleted: gradually
Formatted: Not Highlight
Formatted: Not Highlight
Formatted: Not Highlight
Deleted: 6a
Deleted: At CB, two phases of enhanced surface Chl-*a* were observed: October 2012–May 2013 and October 2013–January 2014, the first corresponding to high biomass and strong organic matter export. …
Formatted: Font: Not Bold
Formatted: Font: Not Bold
Formatted: Font: Bold
Deleted: The second, however, showed decoupling between surface productivity and export: moderate to high export fluxes occurred despite low Chl-*a* in October 2012 and June–September 2013, whereas November 2013–January 2014 featured elevated Chl-*a* but declining export.
Deleted: 6b–CB
Deleted: ¶ ... [3]

Deleted: elevated values
Formatted: Not Highlight
Deleted: s
Deleted: .
Deleted: 6c–CB, 6c–M1
Formatted: Not Highlight
Deleted: ~40 days before trap arrival
Deleted: winter
Deleted: no surface
Deleted: detected
Deleted: the study period
Deleted: s
Deleted: 6d–CB, 6d–M1

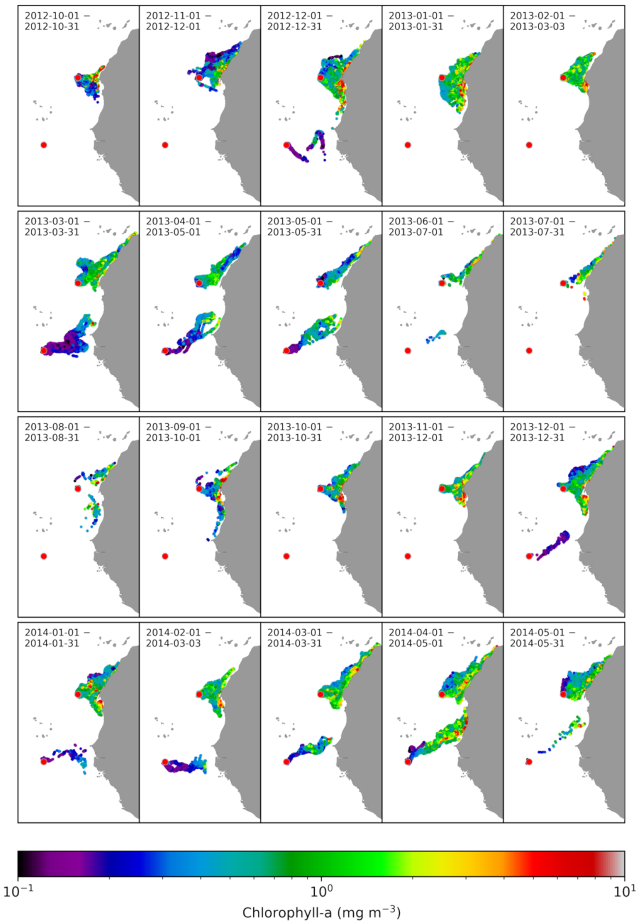

Figure 5: Lagrangian spatiotemporal patterns of Chl-enriched surface water masses tracked from virtual particles seeded from the NW African coast and subsequently advected offshore. Only the trajectories crossing the location of at least one of the trap moorings are included (red dots indicate the location of mooring sites CB and M1). Time intervals coinciding with those of the sediment traps for the studied year are from October 2012 to February 2014.

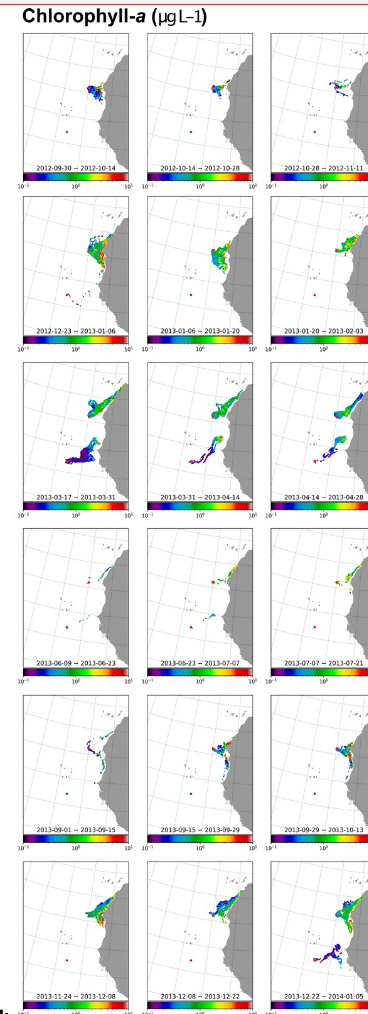

Deleted:

Deleted: a

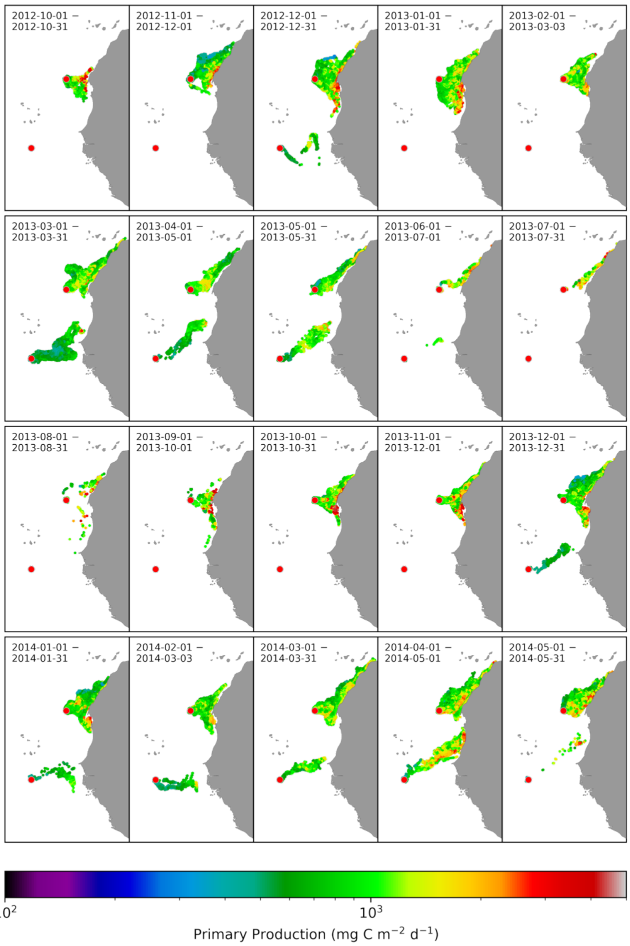

Figure 6: Lagrangian spatiotemporal patterns of PP-enriched surface water masses tracked from virtual particles seeded from the NW African coast and subsequently offshore. Only the trajectories crossing the location of at least one of the trap moorings are included (red dots indicate the location of mooring sites CB and M1). Time intervals coinciding with those of the sediment traps for the studied year are from October 2012 to February 2014.

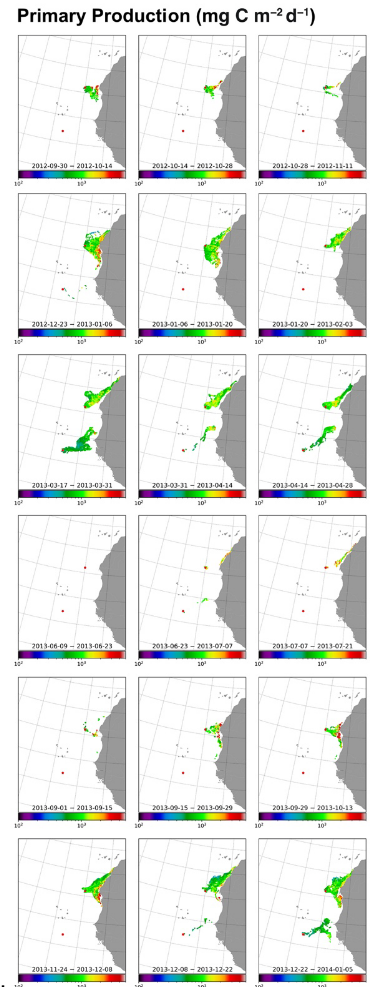

Deleted:

Formatted: English (UK)

Formatted: English (UK)

Deleted: 5b

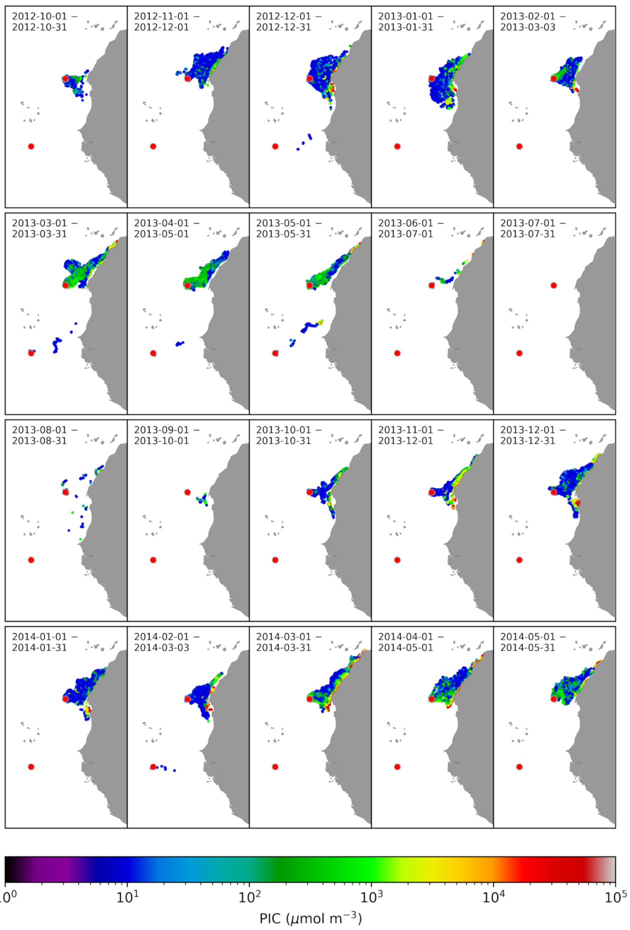

Figure 7: Lagrangian spatiotemporal patterns of PIC-enriched surface water masses tracked from virtual particles seeded from the NW African coast and subsequently advected offshore. Only the trajectories crossing the location of at least one of the trap moorings are included (red dots indicate the location of mooring sites CB and M1). Time intervals coinciding with those of the sediment traps for the studied year are from October 2012 to February 2014.

Deleted:

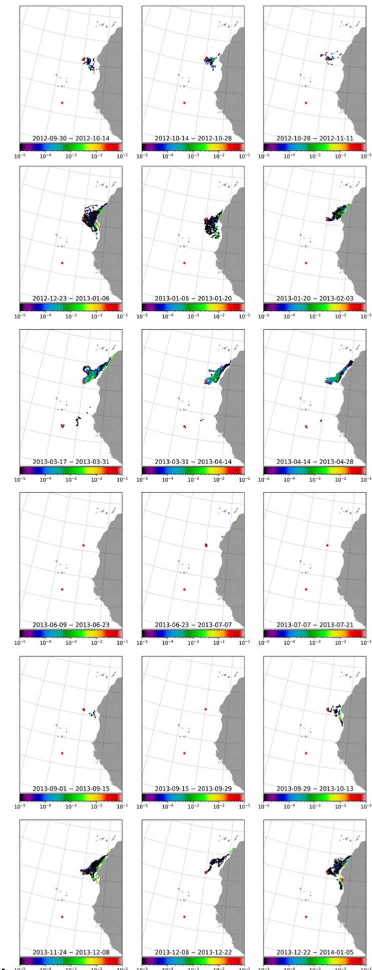

Deleted: 5c

Deleted: e

Deleted: (

Deleted:)

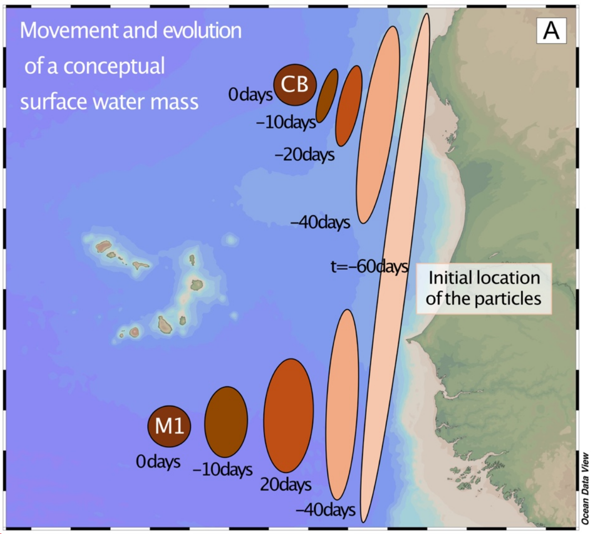

Figure 8a: Schematic representation of the dominant upstream pathways and temporal evolution of water masses reaching each sediment trap, used to link coastal–offshore transport with satellite-derived Chl-*a*, PIC, and PP along their trajectories (Fig. 8b). Pathways were obtained from Lagrangian backtracking of virtual surface particles released off NW Africa and advected in GCM-derived velocity fields.

Deleted:

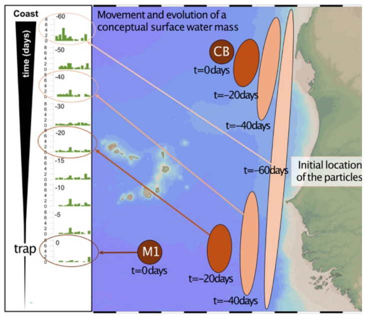

Deleted: 6

Deleted: s

Deleted: 6

Deleted: –d

Formatted: Font: Italic

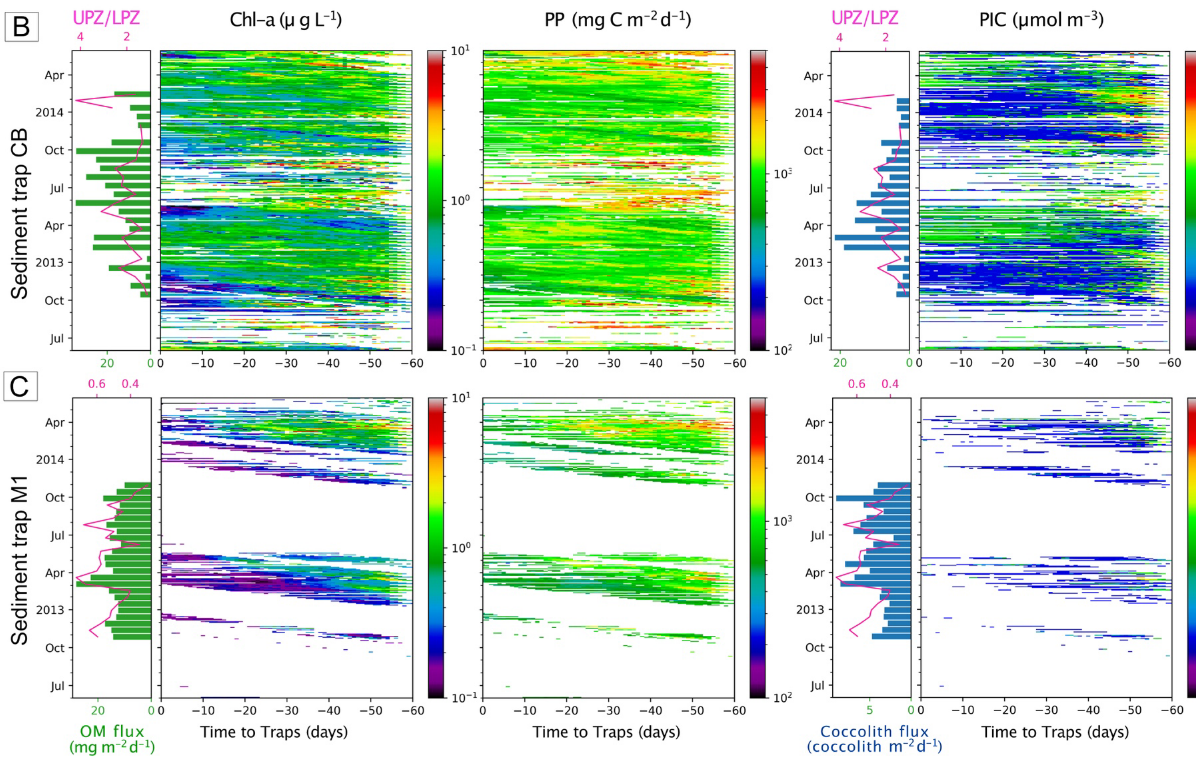

Figure 8b: Organic matter (OM) flux (green bars), coccolith fluxes (coccolith m^{-2} d^{-1}) and coccolith UPZ/LPZ ratios (pink line), collected *in situ* by traps CB (left) and M1 (right) at 1200 m depth (data from Korte et al., 2017; Guerreiro et al., 2019, 2021), alongside Lagrangian-derived, remotely sensed daily Chlorophyll-*a* (Chl-*a*) concentrations, Primary Production (PP) rates, and Particulate Inorganic Carbon (light green bars) at the trap locations (0 days) and back to and 60 days prior to the arrival of virtual particles. Coccolith flux and UPZ/LPZ ratio scales differ between traps.

Deleted: ¶

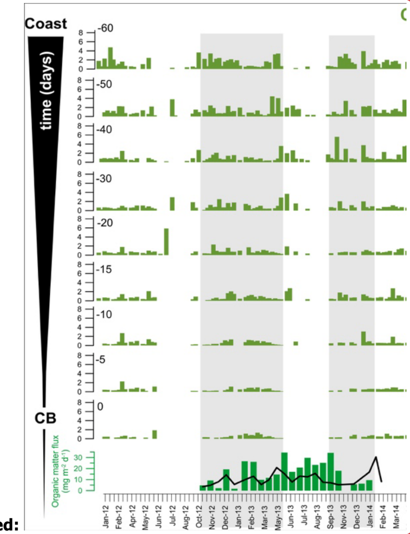

Deleted:

Deleted: and

Formatted: Superscript

Deleted:

Formatted: Font: Italic

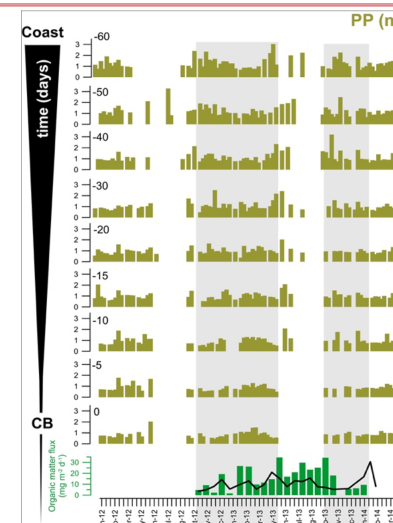

Deleted:

4.5 *In situ* CTD profiling and coccolithophore concentrations in March 2023

Clear environmental contrasts between the CB and M1 mooring regions, already evident from Lagrangian backtracking of remotely-sensed biogeochemical parameters and *in situ* particle fluxes (sections 4.1–4.3), were further confirmed by CTD profiles and extant coccolithophore observations collected in March 2023 during cruise 64PE514-DUST2023 (Figs. 1, 9).

Near M1 (stations ST03 and ST07; 11–13° N, 22° W), surface waters in the upper 40–50 m were warmer (~23.5–25.4 °C), more stratified, and oxygen-poor (~200 µmol L^{-1}) compared to CB (stations ST10 and ST11; 20–21° N, 20–21° W), where surface temperatures were <21 °C and oxygen concentrations exceeded 375 µmol L^{-1}. The fluorescence Chl-*a* (F Chl-*a*) maximum near M1 occurred deeper and was weaker (0.7–1.3 µg L^{-1} at 45–55 m), with lower coccolithophore abundances (maximum 7–10 × 10^3 cells L^{-1}) and UPZ/LPZ ratios than at CB, where the F Chl-*a* maximum was shallower and more intense (1.2–1.4 µg L^{-1} at 21 m) and coccolithophore abundance reached up to seven times higher (16–69 × 10^3 cells L^{-1}).

Among all stations, ST07 (just North of site M1) was the least productive, showing the lowest F Chl-*a*, coccolithophore concentrations, and UPZ/LPZ ratios across the upper 150 m. Interestingly, at the southernmost M1 station (ST03), the F Chl-*a* maximum was deeper but comparable in magnitude to values observed farther north near Cape Blanc (Fig. 9).

Differences in surface F Chl-*a* measured *in situ* with the CTD closely matched daily averaged satellite-derived Chl-*a* concentrations, which ranged from 0.1–0.2 µg L^{-1} at stations ST03 and ST07 near M1, compared to 0.7–1.8 µg L^{-1} at ST10 and ST11 near CB, measured on the same sampling days during the cruise (satellite-driven Chl-*a* sources indicated in Table S1, Supplementary Material).

Deleted: ¶ ... [4]
Formatted: English (UK)
Deleted: —
Formatted: Line spacing: 1,5 lines
Deleted: -
Deleted: —
Formatted: Font: Italic
Deleted: 7
Deleted: 7

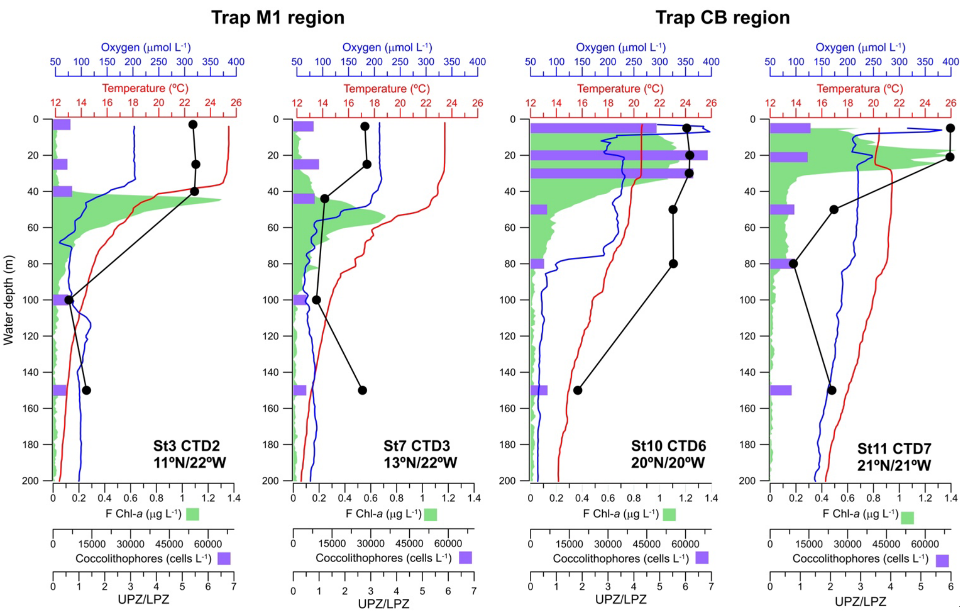

Figure 9: CTD stations near sediment trap moorings M1 (ST03 and ST07) and CB (ST10 and ST11) during expedition PE64514-DUST2023 (6–27 March 2023), at which we measured vertical profiles of temperature, oxygen, and fluorescence-Chla (F-Chla), and quantified the coccolithophore concentrations and UPZ/LPZ ratios along the photic zone of the ocean (Stuut et al., 2023).

5 Discussion

In the central–southern Canary Current EBUS, seasonal variability in coastal primary production, the pathways and magnitude of cross-shelf export, and the offshore flux of biogenic particles were shaped by both large-scale and local atmospheric–hydrographic interactions modulated by trade wind intensity, and therefore sensitive to climate change. Differences in particle-flux magnitude and composition between the two sediment traps, including coccolith assemblages, reflect the extent to which mixed-layer depth dynamics, nutrient supply, and particle sinking rates are influenced by these drivers. These relationships are explored in detail in the following sections.

5.1 Coastal-to-ocean pathways of productive waters in the Canary Current EBUS

All three biogeochemical parameters used in the Lagrangian backtracking analysis (i.e., Chl-*a*, PIC, and PP) showed a steady coast-to-ocean decline, beginning roughly 50–60 days before water masses reached the open-ocean sediment traps (Fig.

Formatted: Normal, Line spacing: Multiple 1,15 li

Deleted: ¶

Deleted: 7

Deleted: ¶ ¶ ¶

Deleted: are

Deleted: ,

Deleted: ,

Deleted: ,

Formatted: English (UK)

Deleted: —

Deleted: —

Deleted: s

8). This pattern persists across seasons, underscoring that although winter–spring trade wind intensification enhances surface mixing and upwelling near the coast, these effects weaken rapidly offshore.

The much steeper offshore declines along trajectories toward M1 compared to persistently higher productivity in coastal and trap-proximal waters at CB (Fig. 8) underscore the role of physical and topographic controls in enhancing the offshore export of organic-rich material off Cape Blanc. These controls include current strength and pathways, mesoscale activity, and shelf geometry (Arístegui et al., 2009; Lovecchio et al., 2018). In contrast, the southern (tropical) and more offshore position of M1, outside the immediate upwelling zone, exposes it to warm, nutrient-poor tropical waters of the southern subtropical North Atlantic gyre (Longhurst, 2006).

Such declines in Chl-*a*, PP and PIC are likely to reflect decreasing nutrient availability, as well as sinking, grazing, remineralisation and aggregation processes that affect particle composition and sinking velocity (e.g., Waniek et al., 2000; van der Jagt et al., 2018). These effects are most pronounced for Chl-*a* and PIC, whereas the rate-based nature of PP results in weaker coast-to-ocean gradients (Fig. 8). In other words, Chl-*a* and PIC represent standing stocks of phytoplankton pigments and particulate calcium carbonate, providing a snapshot of biomass at a given time, whereas PP quantifies the rate of organic carbon fixation through photosynthesis. High calcite sinking rates, in turn, may actually enhance PIC loss toward the open ocean, especially at the more offshore-influenced M1 site.

Beyond identifying the coastal-to-ocean pathways feeding traps CB and M1, the Lagrangian analysis also clarifies how these connections vary seasonally. During the windy, dry months of boreal winter and spring, when the southward shift of the ITCZ strengthened NE trade winds over both CB and M1 (Basha et al., 2015; Guerreiro et al., 2019), CB was primarily influenced by NE-derived coastal waters (Fig. 4), likely carried by a strengthened Canary Current merging into the southwestward NEC (Philander, 2001). This coincided with peak offshore export of chlorophyll-rich waters and elevated PP towards CB (Figs. 5–8), consistent with the combined action of enhanced upwelling, filament formation, frontal intensification, and mesoscale eddy activity along the NW African coast during winter–spring, collectively amplifying surface productivity and cross-shelf export (Arístegui et al., 2009; Meunier et al., 2012; Pelegrí et al., 2017; Hernández-Hernández et al., 2020; Santana-Falcón et al., 2020; Vázquez et al., 2021). High upwelling-index anomalies and low SSH during this period (Fig. 10a) indicate that the dominant drivers were the seasonal intensification of wind-driven upwelling, bringing nutrient-rich SACW to the surface near Cape Blanc, together with mixing associated with enhanced cyclonic eddy activity, consistent with previous studies (Arístegui et al., 2009; Meunier et al., 2012; Pastor et al., 2013). Offshore export of these productive waters was likely further enhanced by lateral advection through the Canary Current–NEC connection and frontal jet intensification along the CVFS (Pastor et al., 2008; Meunier et al., 2012). Combined, these processes have been reported to generate filaments and plumes extending 300–500 km offshore, transporting nutrient-rich waters into the CVFS near Cape Blanc (Pelegrí et al., 2017), while southward-drifting eddies advect high- chlorophyll waters offshore (Barton et al., 2004; Arístegui et al., 2009; Sangrá et al., 2009; Hernández-Hernández et al., 2020).

Despite its more tropical position, outside the core Canary Current pathway, the M1 catchment area was also influenced by NE-sourced waters, likely delivered by offshore advection associated with the NEC, which flows westward

Deleted: 6a–c
Deleted: s
Deleted: 6a–c
Deleted: —
Deleted: efficiency
Deleted: on
Deleted: cross-shelf transport—
Deleted: ing
Deleted: —at collectively enhancing the offshore export of organic-rich material off Cape Blanc
Deleted: ,
Deleted: e
Formatted: Font: Italic
Deleted: —being rate-based—
Formatted: Font: Italic
Deleted: shows
Deleted: s
Deleted: 6b–c
Formatted: Font: Italic
Deleted: inorganic carbon
Formatted: Font: Not Bold
Deleted: 6
Deleted: 8
Deleted: —
Deleted: ing
Deleted: —combined
Deleted: were the dominant drivers,
Deleted: is
Deleted: Chl-*a*
Deleted: , offshore

between ~10–20° N and is fed by the Canary Current (Stramma and Schott, 1999). In line with this connectivity, surface productivity at M1 also peaked in spring 2013, most strongly in March (Figs. 4–8), consistent with previous reports of wind-driven transient mixing generating chlorophyll-rich intrusions during February–May (Kostianoy and Zatsepin, 1996; Arístegui et al., 2009). This typically occurs when the Canary Current–NEC linkage, Ekman upwelling, SACW intrusion, and the CVFS filament system intensify in late winter–spring (Lathuilière et al., 2008; Arístegui et al., 2009; Santana-Falcón et al., 2020), with filament tips, eddies, and the southern CVFS front intermittently injecting productive waters into the M1 region (Meunier et al., 2012; Burgoa et al., 2020). Although upwelling filaments reaching this trap are mostly transient (Kostianoy and Zatsepin, 1996), as reflected by the comparatively lower upwelling index anomalies and less negative SSH compared to CB (Fig. 10a), the Mauritanian–Senegalese coast is nevertheless recognized as one of the most productive sectors of the CCS, sustained by SACW upwelling and additional riverine inputs near the system's southern boundary (Dai and Trenberth, 2002; Karstensen et al., 2008; Brandt et al., 2015). Episodic zonal flows south of Cape Verde (December 2012, March 2013, December 2013–January 2014, February 2014; Figs. 4–7) further suggest that M1 may occasionally receive input from water masses linked to the Guinea Dome, where intensified upwelling and cyclonic circulation can generate eddies that propagate west-northwestward, potentially transporting nutrient-rich waters toward the trap (Pastor et al., 2013).

Despite all these seasonal inputs to M1, the fact that *in situ* measurements from March 2023 show comparable Chl-*a* concentrations at the ~50 m DCM near M1 and in the surface-intensified chlorophyll peak at CB (Fig. 9) does not imply similar biomass production at the two sites. Instead, the elevated but deeper Chl-*a* maximum at M1 is more plausibly explained by photoacclimation, i.e., increased cellular chlorophyll content under low-light, stratified conditions, rather than by equivalent phytoplankton biomass (Poulton et al., 2006; Cullen, 2015).

During the warmer, wetter months of boreal summer and autumn, the northward shift of the ITCZ (~12–15° N) weakened NE trade winds over both trap sites (Basha et al., 2015; Guerreiro et al., 2019). At CB, circulation was dominated by southeast-advected waters (Figs. 4–7) transported by a strengthened poleward Mauritanian Current in response to reduced trade wind forcing during the upwelling relaxation season (Pastor et al., 2012). This current, extending to ~250 m depth (Klenz et al., 2018), advects warm, saline, nutrient-poor waters, and limits cross-shelf export of productive waters along the CVFS (Pastor et al., 2008; Meunier et al., 2012), thus restricting the transport to CB of coastal waters high in Chl-*a*, PIC, and PP during this time of the year (Figs. 5–8). At M1, higher precipitation and SST (Fig. 2) and the absence of wind-driven coastal advection from July–December 2013 (Figs. 4–7) reflected even stronger, longer exposure to ITCZ-driven stratification (Guerreiro et al., 2019) resulting in even lower surface productivity (Fig. 8). Occasional inflows from the ENE/ESE in November and December 2012 may relate to localized upwelling induced by cyclonic wind stress curl (Klenz et al., 2018).

5.2 Coupled variability in surface productivity and deep export fluxes

Deep-ocean sediment-trap moorings provide key constraints on seasonal variability in the biological carbon pump (e.g., Milliman, 1993; Wefer and Fischer, 1993; Baumann et al., 2005; Fischer et al., 2019; Guerreiro et al., 2021) yet directly linking surface productivity to deep-ocean fluxes remains challenging because traps integrate environmental signals over broad spatial

- **Deleted:** —but less prominently than at CB
- **Deleted:** —
- **Deleted:** 6
- **Deleted:** —
- **Deleted:** 8
- **Deleted:** —
- **Deleted:** 5
- **Formatted:** Font: Italic
- **Deleted:** 7
- **Formatted:** Font: Italic
- **Deleted:** —
- **Deleted:** —
- **Formatted:** Font: Not Bold
- **Formatted:** Indent: First line: 1,27 cm
- **Deleted:** 5
- **Deleted:** thus
- **Deleted:** 6
- **Deleted:** 5
- **Deleted:** 6
- **Deleted:** between late October
- **Deleted:** and early January 2013
- **Deleted:** ¶
- **Deleted:** It is worth noticing the strong interannual Chl-*a* variability near M1, with higher surface concentrations close to the trap (~15 days prior) in April 2012 and March–April 2014 compared to the sediment-trap period (Fig. 6b–M1). This suggests that productivity there occasionally exceeded 2013 levels, possibly reflecting the above-average surface warming at M1 during the study period reported by Guerreiro et al. (2019).¶
- **Formatted:** English (UK)

and temporal scales. Combining Lagrangian trajectories, multivariate statistics, and photic-zone observations helps disentangle the drivers of particle-flux variability across the distinct hydrographic settings of CB and M1.

The sharper offshore declines in Chl-*a*, PP, and PIC along trajectories reaching M1 (Section 5.1) are nicely reflected in lower standing stocks of extant coccolithophores and reduced deep-ocean fluxes of coccoliths and total $CaCO_3$ at this site relative to CB (Figs. 2, 8–9; Table S2 – Supplementary Material). These gradients are mirrored in the composition of sinking material: differences in coccolith assemblages and biogenic particle signatures align well with site-specific environmental conditions, as captured by both the Pearson correlations and the PC1 structure, which summarises the dominant environmental axis separating the two stations. Variables associated with productive, well-mixed conditions (i.e., high UPZ/LPZ ratios, elevated Chl-*a*, deeper MLD, and enhanced $CaCO_3$ export, together with contributions from *E. huxleyi*, *C. leptoporus* and satellite-driven PIC) cluster on the positive side of the axis. In contrast, the negative loadings are associated with indicators of warm, stratified waters, including *Helicosphaera* spp. and SST, with further contributions from deep-dwelling taxa and precipitation (Tables 1–2; Fig. 3). Accordingly, positive PC1 scores dominant at CB reflected fast-blooming, placolith-forming communities typical of vigorous upwelling, whereas negative scores dominant at M1 reflected more mesotrophic tropical assemblages shaped by stratification and enhanced precipitation rates associated with greater ITCZ exposure.

These relationships are statistically significant (Table 1) and consistent with the higher and more seasonally variable biogenic fluxes at CB (Fig. 2; Guerreiro et al., 2019) and its stronger coast-to-ocean connectivity revealed by the Lagrangian analysis (Figs. 4–8). The carbonate-rich character of CB, evidenced by higher PIC along upstream trajectories (Section 5.1), is supported by the 1.6× greater coccolith fluxes and 2.4× higher $CaCO_3$ fluxes relative to M1 (Figs. 2c,d; Table S2 – Supplementary Material). Sinking assemblages dominated by fast-blooming (r-selected) coccolithophores, together with photic-zone observations showing up to fourfold higher extant concentrations and elevated UPZ/LPZ ratios at CB under similar March 2023 conditions (Fig. 9), further validate the UPZ/LPZ ratio as a robust indicator of productive, well-mixed waters (Guerreiro et al., 2019) and underscore the more efficient export of coastal high-productivity waters advected toward CB.

The combined datasets confirm that the exceptionally high $CaCO_3$ export at CB reflects persistent upwelling-driven conditions that favour calcifying plankton (e.g., Fischer et al., 2016, 2019; Romero et al., 2020; Guerreiro et al., 2021), likely enhanced by vigorous cross-shelf transport via the Giant Cape Blanc filament (Lovecchio et al., 2018; Hailegeorgis et al., 2021), which carries a large fraction of coastal production offshore (Pelegrí et al., 2005; Álvarez-Salgado et al., 2007; Tilstone et al., 2015; Santana-Falcón et al., 2020). Sinking particles from Cape Blanc can be traced >400 km offshore (Fischer et al., 2007, 2009; Fischer and Karakas, 2009), and models suggest suspended POC may be advected even farther (Lovecchio et al., 2018).

Although pteropods and foraminifers account for a substantial fraction of this high carbonate flux (Guerreiro et al., 2021), consistent with elevated calcifying-zooplankton biomass in EBUS regions (e.g., Knecht et al., 2023), the strong positive

Formatted: Font: 10 pt, English (UK)
Formatted: Font: 10 pt, Italic, English (UK)
Formatted: Font: 10 pt, English (UK)
Deleted: 7
Deleted: .¶
¶
PC1…
Deleted: —
Formatted: Font: Italic, English (UK)
Formatted: English (UK)
Deleted: —
Deleted: side groups
Formatted: English (UK)
Deleted: —
Deleted: —characterize
Deleted: —
Deleted: —correspond to
Deleted: oligo
Deleted: ,
Formatted: English (UK)
Deleted: s
Deleted: due to
Deleted: s
Deleted: 6a–d
Formatted: English (UK)
Deleted: compared with M1
Deleted: 7
Deleted: —
Deleted: —

loadings of coccolith-$CaCO_3$, total $CaCO_3$ and all coccolith taxa on PC2 (Table 2; Fig. 3) indicate that coccolithophores also form a coherent and significant component of total carbonate export at CB during mid-winter and spring. The positive correlation between the UPZ/LPZ ratio and fluxes of coccolith-$CaCO_3$, total $CaCO_3$, and satellite-derived PIC (Tables 1–2; Fig. 3, PC1), together with the fact that *E. huxleyi* was the only variable showing a statistically significant positive correlation with satellite-PIC, further underscores the dominant contribution of surface-dwelling, fast-blooming taxa to carbonate production in the CCS and to the calcite reflectance signal detectable by satellite sensors. Their prominence at CB reflects their ability to thrive under the shallow-nutricline conditions typical of upwelling-influenced waters. In contrast, during more stratified seasons and at offshore settings such as M1, blooms are weaker and substantial calcification occurs deeper in the water column, below the satellite-sensed layer (Guerreiro et al., 2021). These patterns highlight the need to account for hydrographic controls on coccolithophore ecology when interpreting satellite-based estimates of coccolithophore productivity.

At M1, located in a region with weaker upwelling and reduced cross-shelf transport (Figs. 4–8; Section 5.1), biogenic fluxes were concomitantly lower and seasonally more stable (Fig. 2), with mesotrophic *Helicosphaera* spp.-dominated coccolith assemblages being consistent with predominantly oligotrophic conditions punctuated by episodic winter–spring enrichment events (Figs. 2c,d; Table S2 – Supplementary Material). Unexpectedly, mean $bSiO_2$ fluxes were higher at M1 (11 mg m^{-2} d^{-1}) than at CB (5 mg m^{-2} d^{-1}), suggesting enhanced diatom export possibly linked to southward-propagating eddies supplying nutrient-rich waters and promoting the formation of large diatom aggregates with high sinking velocities (Fischer et al., 2021). In addition, the positive association between $bSiO_2$ and dust in the negative PC1 loadings could reflect dust acting either as a source of nutrients and/or as mineral ballast, as discussed in Section 5.3.

Interestingly, all carbonate indicators were negatively correlated with organic matter fluxes (Table 1), particularly during autumn and early winter at CB (Table 2; Fig. 3, PC2), a season marked by higher SST, moderate upwelling, near-zero SSH, and low absolute values of coccolith fluxes, satellite-derived PIC and organic-matter export (Figs. 2, 10). Despite this anti-correlation not being statistically significant, it suggests a shift in the composition of sinking material under these hydrographic conditions. During these months, coccolithophore communities at CB remained dominated by placolith-producing taxa but less productive overall, contributing less to carbonate export, whereas the slight increase in deep-dwelling species suggests a deeper and less favourable photic-zone habitat for UPZ bloomers. Meanwhile, although organic matter export was also reduced in absolute terms, it was likely maintained by these deep-dwelling coccolithophores and other non-blooming phytoplankton, potentially associated with a more prominent DCM, and/or by continued lateral supply of organic-rich material from the coast.

This interpretation is consistent with long-term observations at CB showing that a substantial fraction of deep organic-carbon flux derives from lateral transport within bottom-intensified particle layers, with 40–60% of organic carbon at ~3600 m attributed to material laterally advected from the coastal region (Fischer, Karakas et al., 2009; Fischer et al., 2019). Downslope transport of organic-rich material along density surfaces, consistent with the "particle injection pump" mechanism described

Formatted: Font: Italic
Deleted:
Deleted: more
Deleted: —
Deleted: 6
Deleted: .
Deleted: C
Formatted: English (UK)
Formatted: Font: Italic
Deleted: dominated by tropical species and mesotrophic *Helicosphaera* spp.—are
Deleted: alternating
Deleted: (summer–autumn)
Deleted: and
Deleted: ally
Deleted: enriched (
Deleted:) conditions
Deleted:
Deleted: Surprisingly
Deleted: T
Deleted: and
Deleted: were negatively correlated
Deleted: —
Deleted: 8
Deleted: T
Formatted: English (UK)
Deleted: —still
Deleted: —
Deleted: ed
Deleted: , while
Deleted: indicates
Deleted: ,
Deleted: —although
Deleted: —
Deleted: (e.g.,
Deleted:)

for other EBUS (Boyd et al., 2019), together with possible remobilisation of semi-labile suspended material, likely explains the observed anti-correlation between carbonate and organic matter fluxes. This may also explain why elevated organic matter export during June–September 2013 occurred despite low surface Chl-*a* along upstream trajectories (Fig. 8), suggesting that the exported material did not originate from contemporaneous surface blooms but from subsurface or laterally transported sources.

Deleted: the
Deleted: 6b–CB
Formatted: Font: Italic, English (UK)
Formatted: English (UK)

A comparable pattern was observed at M1 following the strong productivity–export coupling in March 2013, where the subsequent period from April 2013 to January 2014 exhibited sustained high organic matter fluxes despite low surface Chl-*a* (Fig. 8). But given the comparably more offshore position of this station, this was likely related to production within a deeper DCM (~45–55 m at M1 vs. 21 m at CB; Fig. 9), reflecting a higher abundance of photo-adapted tropical phytoplankton communities, typically small eukaryotes, which are common in stratified open-ocean waters and support a persistent DCM under reduced-light conditions (e.g., Cullen, 2015).

Formatted: Font: Italic, English (UK)
Formatted: English (UK)
Deleted: 6b–M1
Deleted: 7
Deleted: —
Deleted: —
Formatted: English (UK)

Overall, the Lagrangian, sediment trap, and photic zone observations show that export fluxes at CB and M1 are not uniformly linked to overlying surface production on seasonal scales but alternate between phases dominated by local productivity and phases driven by laterally advected organic matter, particularly at CB, thereby contributing to resolve when coupling is tight and when subsurface or horizontal processes dominate. Taken together, these patterns also suggest that biogenic carbonate and organic matter fluxes were not always coupled, in contrast with the classical model in which coccoliths and other carbonate particles act as mineral ballast increasing the efficiency of organic carbon export in the tropical NE Atlantic (Ziveri et al., 2007; Guerreiro et al., 2021, 2024; Fischer et al., 2019 and references therein). Instead, our results point to a seasonal alternation in export regimes: carbonate export dominates primarily during the upwelling-driven, high productivity conditions of late winter and spring, whereas organic matter export under the more stable conditions of summer, autumn, and early winter is likely sourced partly from deeper or laterally transported material and/or stimulated by other mechanisms (discussed in section 5.3). This suggests that coccolith-driven ballast is not a persistent mechanism in this part of the central–southern CCS, but one that operates mainly during strong-upwelling phases.

5.3 Upwelling vs. Dust: seasonal drivers of export production

Formatted: English (UK)

Having established the seasonal coupling between surface productivity and deep export in the central–southern CCS, we now examine the relative roles of upwelling and Saharan dust deposition in modulating this variability. As discussed in Section 5.2, both CB and M1 exhibited their highest export production during late winter–spring 2013, with CB showing an additional peak in May–June. These export maxima were tightly coupled to enhanced surface Chl-*a* and PP at CB (Fig. 2), coinciding with the arrival of NE-sourced waters and seasonally intensified mixing, upwelling, and cyclonic eddy activity (Figs. 2, 8). Importantly, these productive periods also coincided with major dust-deposition pulses (Figs. 2e, 10), providing an opportunity to assess the relative influences of dust versus upwelling on export production.

Formatted: English (UK)
Formatted: Font: Italic, English (UK)
Formatted: English (UK)
Deleted: 6a–d, 8a
Deleted: 8

Following these spring peaks, surface biomass declined as trade winds weakened and upwelling relaxed (Fig. 10), while increasing influence of Mauritanian Current waters (Figs. 5–8) produced a shallower, less productive mixed layer (Fig. 2b). Despite these more stratified conditions, CB exhibited unexpectedly high organic-matter fluxes during summer, whereas M1 returned to the lower fluxes typical of pre-March conditions. This period also coincided with renewed Saharan dust deposition, consistent with the seasonal northward migration of the West African dust plume (Adams et al., 2012; Tsamalis et al., 2013; Prospero et al., 2014; Yu et al., 2019) and potentially enhanced by rainfall, especially at M1 (Figs. 2a,e).

Collectively, these observations are consistent with Saharan dust contributing to enhanced export both during the windy, upwelling-influenced season and during the warmer, less productive months. Still, disentangling whether dust acted primarily through fertilisation or through mineral ballasting remains challenging. The Pearson correlations and PC1 loadings show that dust aligns most strongly with warm, stratified conditions and with taxa typical of deeper or mesotrophic photic zones (e.g., *Helicosphaera* spp. and deep-dwellers, more abundant at M1), while consistently anti-correlated with indicators of upper-photic-zone productivity (i.e., Chl-*a*, UPZ/LPZ ratio, mixed-layer deepening and $CaCO_3$ export) (Tables 1–2; Fig. 3). This indicates that dust deposition was statistically more linked to the warmer, more stratified, tropical-like open-ocean conditions at M1, where surface productivity was much lower year-round. PC2 further distinguishes intervals of enhanced coccolith-$CaCO_3$ export from those dominated by organic matter fluxes (Section 5.2), with no clear evidence for dust-stimulated new production.
Since tropical coccolithophores, more abundant at M1, are neither bloom-forming nor known to respond directly to airborne nutrients (Guerreiro et al., 2017; 2023), and given the pronounced mismatch between persistently low surface productivity and high deep organic matter and $bSiO_2$ fluxes at this trap, the data more strongly support Saharan dust acting primarily as a ballasting agent that accelerated the export of pre-existing biogenic material. This is further supported by the sustained summer organic-matter export at CB, which occurred despite low surface Chl-*a*, shallow mixed layers, and relaxed upwelling, but coincided with elevated dust fluxes. This interpretation is consistent with long-term sediment-trap observations at CB by Fischer et al. (2019), who attributed the rapid formation and sinking of dust-ballasted aggregates to the persistent coupling between dust deposition and fluxes of organic matter and $bSiO_2$ under both dry (winter–spring) and wet (summer) depositional regimes over 1988–2016, in line with experimental evidence from the Mauritanian margin (van der Jagt et al., 2018).

While our multivariate statistical analyses argue against dust being a dominant fertilising driver at seasonal scales, the absence of direct measurements of nutrient addition, iron bioavailability, or phytoplankton physiological responses means that the relative importance of fertilisation versus ballasting can only be partially resolved with the present dataset. Furthermore, individual events of enhanced UPZ/LPZ ratios during dust-associated export pulses may show transient fertilisation superimposed on ballasting during both upwelling-driven blooms as well as during the more stratified phase. This was the case

Deleted: 8
Deleted: 6
Formatted: English (UK)
Deleted: —
Deleted: strongly suggest that
Deleted: ed
Formatted: Font: 10 pt, English (UK)
Deleted:
Deleted: —
Deleted: ,
Deleted: , fast-blooming taxa (*E. huxleyi*, *C. leptoporus*
Deleted: , and satellite-derived PIC
Formatted: Font: 10 pt, English (UK)
Formatted: Font: 10 pt, Italic, English (UK)
Formatted: Font: 10 pt, English (UK)
Deleted: compared to CB
Deleted: These patterns are inconsistent with nutrient-driven fertilisation, which would require positive correlations with surface productivity indicators.¶
Deleted: —
Deleted: —
Deleted: suggest
Formatted: Font: Italic, English (UK)
Formatted: English (UK)
Formatted: English (UK)
Deleted: lithogenic
Deleted: —a combination that is difficult to reconcile with nutrient fertilisation and instead points to dust acting mainly through mineral ballasting and/or lateral or subsurface supply of previously produced organic matter (Section 5.2).
Formatted: English (UK)
Deleted: reported
Deleted: fluxes
Formatted: English (UK)
Deleted: , attributed to rapid formation and sinking of dust-ballasted aggregates
Deleted: Despite our multivariate statistical analyses arguing against dust being a dominant fertilising driver at seasonal scales,
Formatted: English (UK)
Deleted: to
Deleted: is

in February–March at both traps, in late July and early September at M1, and in May and July–August at CB (Fig. 10), suggesting species-specific responses to atmospheric inputs under both dry and wet depositional regimes. While episodic dust intrusions may have enhanced export at both sites primarily through ballasting, a fertilisation contribution cannot be fully ruled out, particularly during summer–autumn when UPZ/LPZ ratios increased sharply at both trap locations despite weakened or suppressed upwelling. This interpretation is consistent with recent evidence of dust-stimulated fast-blooming species *E. huxleyi* and *Gephyrocapsa oceanica* together with N_2-fixing diazotrophic *Trichodesmium* sp. in the tropical NE Atlantic (AMT28; Brotas et al., 2023; Guerreiro et al., 2023), with earlier sediment-trap records documenting sharp increases in POC, placolith coccoliths, UPZ/LPZ ratios, and coccolith Sr/Ca ratios during dust events in stratified tropical waters (Guerreiro et al., 2017, 2024), and with long-term satellite-derived co-occurring AOD and Chl-*a* maxima downwind of NW African dust sources (Guerreiro et al., 2023). Additional direct observations combining higher-resolution sediment-trap records with time-series measurements from dust collectors at the surface and seawater biogeochemical properties across the photic zone, including e.g. particle aggregate composition analyses, and measurements of dust-associated nutrient and trace-metal fluxes, would however be required to more conclusively disentangle fertilization from mineral-ballasting effects.

Interestingly, the relationship between AOD and measured dust fluxes was not statistically significant and only weakly positive in both the Pearson correlation and PC1 results (Tables 1 and 2; Fig. 3). This likely reflects seasonal differences in atmospheric transport and deposition: satellite-derived AOD is highest under dry, cloud-free conditions, whereas during periods of rainfall the associated cloud cover prevents reliable AOD retrievals and thus suppresses the satellite AOD signal despite enhancing dust fluxes (Korte et al., 2017; Guerreiro et al., 2017; van der Does et al., 2021). This mismatch was especially pronounced in summer–autumn at both sites, when stronger ITCZ influence increased wet dust deposition while simultaneously reducing AOD visibility.

Finally, several dust-related export peaks coincided with sharp declines in the rain ratio (Fig. 2d,e), suggesting increased efficiency of the biological carbon pump—a pattern also observed in the western tropical North Atlantic (Guerreiro et al., 2021). At CB, this occurred in late May, late July, and late September 2013, whereas the highly productive late winter 2013 event partially diverged from this pattern, with March showing elevated rain ratios suggesting enhanced calcification offsetting carbon sequestration. Similar though weaker dust-related increases in rain ratios occurred at M1 during March and late July 2013. These results suggest that dust impacts on the biological carbon pump are not uniform but species- and regime-dependent.

Overall, despite separating dust from upwelling influences remaining complex, our data suggest a synergistic interplay between atmospheric deposition and oceanic forcing in sustaining high productivity an export across the central–southern Canary Current EBUS. These findings underscore the need for long-term *in situ* time series to disentangle physical–biogeochemical

Deleted: supported by enhanced UPZ/LPZ ratios during dust-associated export pulses (

Deleted: ;

Deleted: ;

Deleted: ;

Deleted: 8

Formatted: English (UK)

Formatted: English (UK)

Deleted: assumption

Formatted: Font: Italic

Deleted: coccolithophore fast-bloomers and

Deleted: s

Formatted: Font: Italic

Formatted: Font: Italic

Formatted: English (UK)

Deleted: and

Formatted: English (UK)

Deleted: ocorring

Formatted: English (UK)

Formatted: Not Highlight

Formatted: Not Highlight

Formatted: Font: Italic

coupling in the Canary Current EBUS, critical for improving model projections of how climate-driven changes in dust supply, warming-induced stratification, and coastal upwelling will shape the ocean's biological carbon pump.

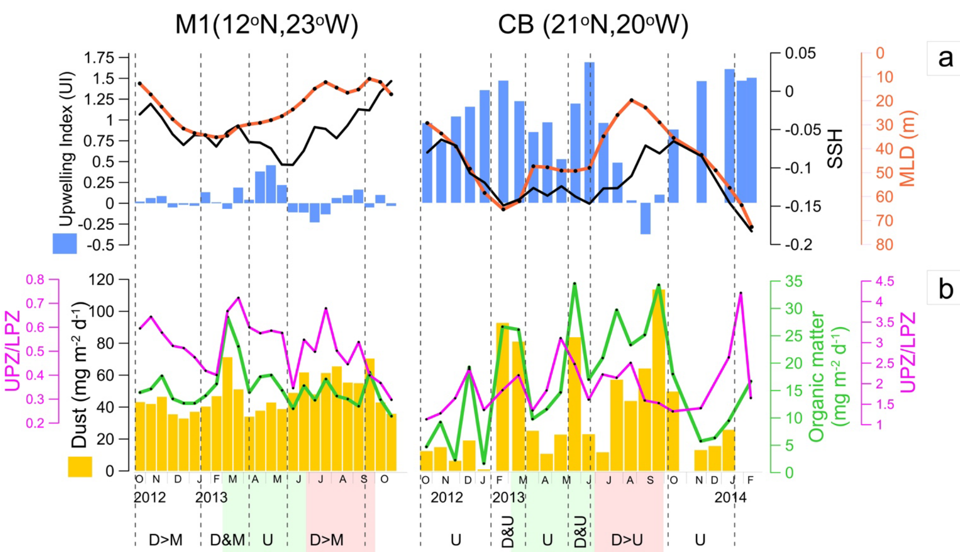

Figure 10: Variation of the (a) SST-based wind-based upwelling index (blue bars), sea surface height (SSH, black line) and mixed layer depth (MLD, orange line), and (b) fluxes of organic matter (green line), dust (i.e., lithogenic flux; orange bars), and coccolith-UPZ/LPZ (pink line) at traps M1 and CB. Vertical panels represent spring (light green) and summer (light pink) seasons. D = Dust, M = Mixing, and U = Upwelling. Particle flux data from Korte et al. (2017), Guerreiro et al. (2019, 2021).

6 Conclusions

This study combines Lagrangian backtracking, satellite observations, photic-zone measurements, and seasonally resolved sediment-trap fluxes to clarify how surface circulation, atmospheric deposition, and subsurface particle sources jointly regulate particle export in the dust-influenced central–southern CCS. Together, these datasets reveal a strong interplay between upwelling-driven nutrient supply, cross-shelf transport, Saharan dust deposition, and lateral or subsurface particle contributions.

Formatted: English (UK)

Formatted: English (UK)

Formatted: English (UK)

Deleted: 8

Deleted: particles

Formatted: English (UK)

Formatted: English (UK), Not Highlight

Formatted: English (UK)

Formatted: English (UK), Not Highlight

Formatted: Not Highlight

Formatted: English (UK)

Deleted: Interestingly, the relationship between AOD and measured dust fluxes was not significant and only weakly positive in both the Pearson correlation and PC1 results (Tables 1 and 2; Fig. 3). This likely reflects seasonal differences in atmospheric transport and deposition: satellite-derived AOD is highest under dry, cloud-free conditions, whereas during periods of rainfall the associated cloud cover prevents reliable AOD retrievals and thus suppresses the satellite AOD signal despite enhancing dust fluxes (Korte et al., 2017; Guerreiro et al., 2017; van der Does et al., 2021). This mismatch was especially pronounced in summer–autumn at both sites, when stronger ITCZ influence increased wet dust deposition while simultaneously reducing AOD visibility.¶
¶
Finally, several dust-related export peaks coincided with sharp declines in the rain ratio (Fig. 2d,e), suggesting increased efficiency of the biological carbon pump—a pattern also observed in the western tropical North Atlantic (Guerreiro et al., 2021). At CB, this occurred in late May, late July, and late September 2013, whereas the highly productive February–March 2013 event partially diverged from this pattern, with March showing elevated rain ratios suggesting enhanced calcification offsetting carbon sequestration. Similar though weaker dust-related increases in rain ratios occurred at M1 during March and late July 2013. These results suggest that dust impacts on the biological carbon pump are not uniform but species- and regime-dependent.¶
¶
Overall, despite separating dust from upwelling influences remaining complex, our data suggest a synergistic interplay between atmospheric deposition and oceanic forcing in sustaining high productivity an export across the central–southern Canary Current EBUS. These findings underscore the need for long-term in-situ time series to disentangle physical–biogeochemical coupling in the Canary Current EBUS—critical for improving model projections of how climate-driven changes in dust supply, warming-induced stratification, and coastal upwelling will shape the ocean's biological carbon pump.¶

Formatted: English (UK)

Coast-to-ocean gradients and site-specific export regimes. Across all seasons, Lagrangian trajectories revealed strong coast-to-open-ocean declines in Chl-*a*, PP, and PIC, with the steepest gradients along pathways to M1. These patterns indicate progressively weaker cross-shelf transfer and a stronger influence of warm, stratified tropical waters at the more offshore M1 location. The imprint of these gradients is evident in the sediment trap record: CB exhibited higher maxima and more temporally variable export, with coccolith sinking assemblages dominated by surface-dwelling, fast-blooming coccolithophores, whereas M1 showed lower but steadier biogenic fluxes enriched in oligo- to mesotrophic tropical taxa, and deep-dwelling species.

Formatted: Font: Italic, English (UK)

Formatted: English (UK)

Seasonal water pathways and winter–spring productivity peaks. Superimposed on these broad gradients, surface water trajectories displayed marked seasonality driven by meridional ITCZ migration and fluctuations in trade wind intensity. During winter–spring, intensified NE trade winds and stronger filament/eddy activity increased the delivery of NE-sourced coastal waters to both traps, particularly to CB, supporting elevated Chl-*a*, PP, PIC, and coccolith-$CaCO_3$ export. Conversely, M1's more tropical, offshore setting limited its connectivity to these productive pathways, resulting in more intermittent upwelling influence and consequently lower, more stable particle and coccolith fluxes across the year.

Deleted: —

Deleted: —

Formatted: Font: Italic, English (UK)

Formatted: English (UK)

Seasonal variability in surface–export coupling. Export was not uniformly linked to contemporaneous surface productivity: coupling was strong during the late winter–spring productive season but weakened markedly thereafter. During the March 2013 productivity peak, both traps showed tight alignment between elevated Chl-*a*, PP, UPZ/LPZ ratios, and enhanced biogenic fluxes, reflecting efficient transfer of newly produced material to depth. In contrast, summer–autumn–early winter at CB, characterised by warmer SST, moderate upwelling, and near-zero SSH, exhibited reduced placolith export yet sustained organic-matter fluxes, consistent with enhanced lateral and subsurface particle supply. At M1, deep ocean fluxes persisted well beyond surface productivity maxima, likely supported by a deeper DCM and photoacclimated tropical communities. Together, these patterns reveal alternating export regimes: phases dominated by local surface production during the productive season, and phases when lateral or subsurface sources become the primary contributors to deep export.

Formatted: Font: Italic

Deleted: —

Deleted: —

Formatted: English (UK)

Dust as a dominant seasonal ballast with episodic fertilisation. Saharan dust contributed substantially to export during both windy late-winter–spring and stratified summer–autumn. Multivariate analyses indicate strong covariance between dust and warm, stratified conditions dominated by tropical taxa, coupled with negative relationships between dust and all upper photic zone productivity indicators, consistent with mineral ballasting as the prevailing dust effect. Nevertheless, several dust-associated export pulses coincided with elevated UPZ/LPZ ratios, suggesting that episodic fertilisation responses by fast-blooming coccolithophores also contributed to enhanced export under both upwelling-driven and stratified conditions.

Deleted: —

Deleted: indicating episodic fertilisation responses by fast-blooming coccolithophores superimposed upon a primarily ballasting-driven regime. ¶

AOD–dust flux decoupling under wet deposition. The weak correspondence between AOD and measured dust fluxes is likely to reflect the suppression of satellite AOD retrievals by cloud cover during wet deposition events, particularly under stronger ITCZ influence during summer–autumn, when wet scavenging enhances downward dust flux while masking the atmospheric signal. This underscores that AOD-based approaches may not fully resolve deposition dynamics across seasons, and therefore benefit from integration with *in situ* measurements.

A dual physical–atmospheric control of export. Overall, the findings demonstrate that winter–spring export in the central–southern CCS is sustained primarily by upwelling-driven nutrient inputs and cross-shelf advection, whereas summer–autumn export is maintained by Saharan dust deposition together with lateral and subsurface particle supply under stronger stratification. These insights contribute to refine mechanistic understanding of export pathways in dusty upwelling systems and highlight the need for sustained, high-resolution time series to project how future changes in dust supply, stratification, and upwelling intensity will shape the biological carbon pump.

Deleted: ballasting

Author contribution

CVG and BJ conceived the study and led the conceptual development, and CVG wrote the manuscript with input from all co-authors. CVG also undertook and supervised the light-microscope analyses of the extant coccolithophore communities shown in Fig. 9. BJ performed the Lagrangian backtracking analysis and produced Figs. 4–8. PL generated the satellite-derived primary production fields and computed the SST-based upwelling index. AF processed all satellite remote-sensing datasets used in the multivariate statistical analysis. All authors contributed to scientific interpretation, reviewed the manuscript, and approved the final version.

Formatted: English (UK)

Deleted: 7

Deleted: 6a

Competing interests

The authors declare that they have no conflict of interest.

Acknowledgements

Formatted: English (UK)

All authors thank the European Space Agency (ESA) for supporting the *4D Atlantic Primary Productivity in Upwelling Ecosystems* (PRIMUS) project (ESA Contract No. 4000135025/21/I-NB). We specifically acknowledge guidance and advice throughout the project from ESA Technical Officers Jérôme Benveniste, Roberto Sabia and Javier Alonso Concha. We also acknowledge use of data previously obtained, processed and stored at PML by the NERC EO Data Analysis and Artificial-intelligence Service (NEODAAS).

Formatted: English (UK)

Coccolith analyses from both moorings and their integration with particle-flux datasets were undertaken within two Marie Skłodowska-Curie Fellowships (MSCA COFUND Grant No. 600411 and MSCA-IF-2017 European Fellowship Grant No.

796802) and a CEECIND Individual Contract awarded to C. V. Guerreiro. All the flux data has been previously published and available at PANGAEA (Korte et al., 2017; Guerreiro et al., 2019, 2021). Extant coccolithophore data from stations 3, 7, 10, and 11 were produced at the Laboratory of Calcareous Nannoplankton (Nanolab–IDL) during Alessia Bataglino's EU-funded Erasmus+ traineeship (University of Milano–Bicocca and CIÊNCIAS ULisboa), supervised by C. V. Guerreiro, within the CHASE project (*CHASing the environmental Effects of dust deposition across the Atlantic and Southern Ocean*).

We thank the captains, crews, and technical teams of cruises RV Meteor M89**,** RV Pelagia 64PE378**,** RV Poseidon POS425, POS445, POS464, and RV Pelagia PE64514, as well as the technicians from NIOZ and MARUM, for their invaluable support in sample and data collection. Mooring M1 was operated by NIOZ under the TRAFFIC (NWO Grant No. 822.01.008) and DUSTTRAFFIC (ERC Grant No. 311152) projects coordinated by Jan-Berend W. Stuut. Moorings CB-23 and CB-24 were operated by Gerhard Fischer within MARUM project GB1 (*Particle flux, carbon turnover and nutrient regeneration*).

Portions of the manuscript benefited from language editing and text refinement of author-written text using an AI-assisted tool (ChatGPT). All scientific interpretation, data analysis, figures and conclusions are the sole responsibility of the authors.

Financial support

This work was financially supported by the European Space Agency through the PRIMUS project (ESA Contract No. 4000135025/21/I-NB). B. Jonsson received additional support from NASA grants 80NSSC21K0563 (Lagrangian analyses of ocean color) and 80LARC21DA002 (GLIMR). C.V. Guerreiro was supported by two Marie Skłodowska-Curie Fellowships (MSCA COFUND Grant No. 600411; MSCA-IF-2017 Grant No. 796802) and by a CEECIND Individual Contract funded by Fundação para a Ciência e a Tecnologia (FCT) (Grant No. CEECIND/00752/2018/CP1534/CT0011; https://doi.org/10.54499/CEECIND/00752/2018/CP1534/CT0011). Extant coccolithophore observations were further supported by an EU Erasmus+ traineeship and by the CHASE project (www.chase-dust.com) at the Laboratory of Calcareous Nannofossils (IDL), with institutional support from FCT, I.P./MCTES (PT) through national funds (PIDDAC): LA/P/0068/2020 (https://doi.org/10.54499/LA/P/0068/2020), UID/50019/2025 (https://doi.org/10.54499/UID/50019/2025), and by the EU (NextGenerationEU) under projects UID/PRR/50019/2025 (https://doi.org/10.54499/UID/PRR/50019/2025) and UID/PRR2/50019/2025 (https://doi.org/10.54499/UID/PRR2/50019/2025. MARE/ARNET also receives support from FCT, through UID/04292/2025 (https://doi.org/10.54499/UID/04292/2025) and LA/P/0069/2020 (https://doi.org/10.54499/LA/P/0069/2020). Data collection and mooring operations at M1 were funded by the NWO TRAFFIC project (Grant No. 822.01.008) and the ERC DUSTTRAFFIC project (Grant No. 311152). Mooring operations at Cape Blanc were supported by the MARUM project GB1.

Deleted: FCUL

Formatted: Space Before: 0 pt, After: 0 pt

Deleted: doi.org/10.54499/CEECIND/00752/2018/CP1534/CT0011

Deleted: .

Formatted: Font: Not Bold, Font colour: Auto, English (UK)

References

Adams, A. M., Prospero, J. M., and Zhang, C.: CALIPSO-Derived Three-Dimensional Structure of Aerosol over the Atlantic Basin and Adjacent Continents, Journal of Climate, 25, 6862-6879, https://doi.org/10.1175/JCLI-D-11-00672.1, 2012.

Alonso-González, I. J., Arístegui, J., Vilas, J. C., and Hernández-Guerra, A.: Lateral POC transport and consumption in surface and deep waters of the Canary Current region: A box model study, Global Biogeochemical Cycles, 23, https://doi.org/10.1029/2008GB003185, 2009.

Álvarez-Salgado, X. A. Arístegui, J., Barton, E. D., & Hansell, D. A.: Contribution of upwelling filaments to offshore carbon export in the subtropical Northeast Atlantic Ocean, Limnology and Oceanography, 52, 1287-1292, https://doi.org/10.4319/lo.2007.52.3.1287, 2007.

Arístegui, J., Barton, E. D., Álvarez-Salgado, X. A., Santos, A. M. P., Figueiras, F. G., Kifani, S., Hernández-León, S., Mason, E., Machú, E., and Demarcq, H.: Sub-regional ecosystem variability in the Canary Current upwelling, Progress in Oceanography, 83, 33-48, https://doi.org/10.1016/j.pocean.2009.07.031, 2009.

Baker, A. R., Adams, C., Bell, T. G., Jickells, T. D., and Ganzeveld, L.: Estimation of atmospheric nutrient inputs to the Atlantic Ocean from 50°N to 50°S based on large-scale field sampling: Iron and other dust-associated elements, Global Biogeochemical Cycles, 27, 755-767, https://doi.org/10.1002/gbc.20062, 2013.

Baker, A. R., Kelly, S. D., Biswas, K. F., Witt, M., and Jickells, T. D.: Atmospheric deposition of nutrients to the Atlantic Ocean, Geophysical Research Letters, 30, https://doi.org/10.1029/2003gl018518, 2003.

Baker, A. R., Weston, K., Kelly, S. D., Voss, M., Streu, P., and Cape, J. N.: Dry and wet deposition of nutrients from the tropical Atlantic atmosphere: Links to primary productivity and nitrogen fixation, Deep Sea Research Part I: Oceanographic Research Papers, 54, 1704-1720, https://doi.org/10.1016/j.dsr.2007.07.001, 2007.

Balch, W. M., Gordon, H. R., Bowler, B. C., Drapeau, D. T., and Booth, E. S.: Calcium carbonate measurements in the surface global ocean based on Moderate-Resolution Imaging Spectroradiometer data, Journal of Geophysical Research: Oceans, 110, https://doi.org/10.1029/2004JC002560, 2005.

Balch, W. M., Drapeau, D. T., Poulton, N., Archer, S. D., Cartisano, C., Burnell, C., and Godrijan, J.: Osmotrophy of dissolved organic compounds by coccolithophore populations: Fixation into particulate organic and inorganic carbon, Science Advances, 9, eadf6973, https://doi.org/10.1126/sciadv.adf6973, 2023.

Barton, E. D.: Meanders, eddies and intrusions in the thermohaline front off Northwest Africa, Oceanologica Acta, 10, 267-283, 1987.

Barton, E. D., Arístegui, J., Tett, P., and Navarro-Pérez, E.: Variability in the Canary Islands area of filament-eddy exchanges, Progress in Oceanography, 62, 71-94, https://doi.org/10.1016/j.pocean.2004.07.003, 2004.

Basha, G., Kishore, P., Venkat Ratnam, M., Ouarda, T. B. M. J., Velicogna, I., and Sutterley, T.: Vertical and latitudinal variation of the intertropical convergence zone derived using GPS radio occultation measurements, Remote Sensing of Environment, 163, 262-269, https://doi.org/10.1016/j.rse.2015.03.024, 2015.

Deleted: ¶
Álvarez-Salgado, X. A.: Contribution of upwelling filaments to offshore carbon export in the subtropical Northeast Atlantic Ocean, Limnology and Oceanography, 52, 1287-1292, https://doi.org/10.4319/lo.2007.52.3.1287, 2007.¶

Formatted: Check spelling and grammar

Baumann, K.-H. and Freitag, T.: Pleistocene fluctuations in the northern Benguela Current system as revealed by coccolith assemblages, Marine Micropaleontology, 52, 195-215, https://doi.org/10.1016/j.marmicro.2004.04.011, 2004.

Baumann, K.-H., Andruleit, H., Böckel, B., Geisen, M., and Kinkel, H.: The significance of extant coccolithophores as indicators of ocean water masses, surface water temperature, and paleoproductivity: a review, Paläontologische Zeitschrift, 79, 93-112, 2005.

Ben-Ami, Y., Koren, I., Altaratz, O., Kostinski, A., and Lehahn, Y.: Discernible rhythm in the spatio/temporal distributions of transatlantic dust, Atmos. Chem. Phys., 12, 2253-2262, https://doi.org/10.5194/acp-12-2253-2012, 2012.

Bergquist, B. A. and Boyle, E. A.: Dissolved iron in the tropical and subtropical Atlantic Ocean, Global Biogeochemical Cycles, 20, n/a-n/a, https://doi.org/10.1029/2005GB002505, 2006.

Brandt, P., Bange, H. W., Banyte, D., Dengler, M., Didwischus, S. H., Fischer, T., Greatbatch, R. J., Hahn, J., Kanzow, T., Karstensen, J., Körtzinger, A., Krahmann, G., Schmidtko, S., Stramma, L., Tanhua, T., and Visbeck, M.: On the role of circulation and mixing in the ventilation of oxygen minimum zones with a focus on the eastern tropical North Atlantic, Biogeosciences, 12, 489-512, https://doi.org/10.5194/bg-12-489-2015, 2015.

Brotas, V., Ferreira, A., Veloso, V., Tracana, A., Guerreiro, C. V., Tarran, G. A., Woodward, E. M. S., Ribeiro, L., Netting, J., Clewley, D., and Groom, S. B.: Assessing phytoplankton community composition in the Atlantic Ocean from *in situ* and satellite observations, Frontiers in Marine Science, Volume 10 - 2023, https://doi.org/10.3389/fmars.2023.1229692, 2023.

Burgoa, N., Machín, F., Marrero-Díaz, Á., Rodríguez-Santana, Á., Martínez-Marrero, A., Arístegui, J., and Duarte, C. M.: Mass, nutrients and dissolved organic carbon (DOC) lateral transports off northwest Africa during fall 2002 and spring 2003, Ocean Sci., 16, 483-511, https://doi.org/10.5194/os-16-483-2020, 2020.

Cermeño, P., Dutkiewicz, S., Harris, R. P., Follows, M., Schofield, O., and Falkowski, P. G.: The role of nutricline depth in regulating the ocean carbon cycle, Proceedings of the National Academy of Sciences, 105, 20344-20349, https://doi.org/10.1073/pnas.0811302106, 2008.

Cullen, J.J.: Subsurface Chlorophyll Maximum Layers: Enduring Enigma or Mystery Solved? Annual Review of Marine Science 7, 207–39, https://doi.org/10.1146/annurev-marine-010213-135111, 2015.

Dai, A. and Trenberth, K. E.: Estimates of Freshwater Discharge from Continents: Latitudinal and Seasonal Variations, Journal of Hydrometeorology, 3, 660-687, https://doi.org/10.1175/1525-7541(2002)003<0660:EOFDFC>2.0.CO;2, 2002.

Dutkiewicz, S., Scott, J. R., and Follows, M. J.: Winners and losers: Ecological and biogeochemical changes in a warming ocean, Global Biogeochemical Cycles, 27, 463-477, https://doi.org/10.1002/gbc.20042, 2013.

Emery, W. J. and Meincke, J. P.: Global water masses: summary and review, Oceanologica Acta, 9, 383-391, 1986.

England, M. H., Li, Z., Huguenin, M. F., Kiss, A. E., Sen Gupta, A., Holmes, R. M., and Rahmstorf, S.: Drivers of the extreme North Atlantic marine heatwave during 2023, Nature, 642, 636-643, https://doi.org/10.1038/s41586-025-08903-5, 2025.

Fiedler, B., Grundle, D. S., Schütte, F., Karstensen, J., Löscher, C. R., Hauss, H., Wagner, H., Loginova, A., Kiko, R., Silva, P., Tanhua, T., and Körtzinger, A.: Oxygen utilization and downward carbon flux in an oxygen-depleted eddy in the eastern tropical North Atlantic, Biogeosciences, 13, 5633-5647, https://doi.org/10.5194/bg-13-5633-2016, 2016.

Formatted: Font: Italic

Deleted: ,

Filipsson, H. L., Romero, O. E., Stuut, J.-B. W., and Donner, B.: Relationships between primary productivity and bottom-water oxygenation off northwest Africa during the last deglaciation, Journal of Quaternary Science, 26, 448-456, https://doi.org/10.1002/jqs.1473, 2011.

Fischer, G.: Report and preliminary results of RV POSEIDON Cruise P425. Las Palmas - Las Palmas, 16.01.2012 - 30.01.2012, 2012.

Fischer, G.: Report and preliminary results of R/V POSEIDON cruise POS445. Las Palmas - Las Palmas, 19.01.2013 01.02.2013, 2013.

Fischer, G.: Report and preliminary results of R/V POSEIDON cruise POS464, Las Palmas (Canary Islands) - Las Palmas (Canary Islands), 03.02.2014 - 18.02.2014, 2014.

Fischer, G. and Karakas, G.: Sinking rates and ballast composition of particles in the Atlantic Ocean: implications for the organic carbon fluxes to the deep ocean, Biogeosciences, 6, 85-102, 2009.

Fischer, G., Reuter, C., Karakas, G., Nowald, N., and Wefer, G.: Offshore advection of particles within the Cape Blanc filament, Mauritania: Results from observational and modelling studies, Progress In Oceanography, 83, 322-330, https://doi.org/10.1016/j.pocean.2009.07.023, 2009.

Fischer, G., Romero, O. E., Karstensen, J., Baumann, K. H., Moradi, N., Iversen, M., Ruhland, G., Klann, M., and Körtzinger, A.: Seasonal flux patterns and carbon transport from low-oxygen eddies at the Cape Verde Ocean Observatory: lessons learned from a time series sediment trap study (2009–2016), Biogeosciences, 18, 6479-6500, https://doi.org/10.5194/bg-18-6479-2021, 2021.

Fischer, G., Karakas, G., Blaas, M., Ratmeyer, V., Nowald, N., Schlitzer, R., Helmke, P., Davenport, R., Donner, B., Neuer, S., and Wefer, G.: Mineral ballast and particle settling rates in the coastal upwelling system off NW Africa and the South Atlantic, International Journal of Earth Sciences, https://doi.org/10.1007/s00531-007-0234-7, 2007.

Fischer, G., Romero, O., Toby, E., Iversen, M., Donner, B., Mollenhauer, G., Nowald, N., Ruhland, G., Klann, M., Hamady, B., and Wefer, G.: Changes in the Dust-Influenced Biological Carbon Pump in the Canary Current System: Implications From a Coastal and an Offshore Sediment Trap Record Off Cape Blanc, Mauritania, Global Biogeochemical Cycles, 33, 1100-1128, https://doi.org/10.1029/2019GB006194, 2019.

Fomba, K. W., Müller, K., van Pinxteren, D., Poulain, L., van Pinxteren, M., and Herrmann, H.: Long-term chemical characterization of tropical and marine aerosols at the Cape Verde Atmospheric Observatory (CVAO) from 2007 to 2011, Atmos. Chem. Phys., 14, 8883-8904, https://doi.org/10.5194/acp-14-8883-2014, 2014.

Friedlingstein, P., O'Sullivan, M., Jones, M. W., Andrew, R. M., Gregor, L., Hauck, J., Le Quéré, C., Luijkx, I. T., Olsen, A., Peters, G. P., Peters, W., Pongratz, J., Schwingshackl, C., Sitch, S., Canadell, J. G., Ciais, P., Jackson, R. B., Alin, S. R., Alkama, R., Arneth, A., Arora, V. K., Bates, N. R., Becker, M., Bellouin, N., Bittig, H. C., Bopp, L., Chevallier, F., Chini, L. P., Cronin, M., Evans, W., Falk, S., Feely, R. A., Gasser, T., Gehlen, M., Gkritzalis, T., Gloege, L., Grassi, G., Gruber, N., Gürses, O., Harris, I., Hefner, M., Houghton, R. A., Hurtt, G. C., Iida, Y., Ilyina, T., Jain, A. K., Jersild, A., Kadono, K., Kato, E., Kennedy, D., Klein Goldewijk, K., Knauer, J., Korsbakken, J. I., Landschützer, P., Lefèvre, N., Lindsay, K., Liu, J., Liu, Z., Marland, G., Mayot, N., McGrath, M. J., Metzl, N., Monacci, N. M., Munro, D. R., Nakaoka, S. I., Niwa, Y., O'Brien, K., Ono, T., Palmer, P. I., Pan, N., Pierrot, D., Pocock, K., Poulter, B., Resplandy, L., Robertson, E., Rödenbeck, C., Rodriguez, C., Rosan, T. M., Schwinger, J., Séférian, R., Shutler, J. D., Skjelvan, I., Steinhoff, T., Sun, Q., Sutton, A. J., Sweeney, C., Takao, S., Tanhua, T., Tans, P. P., Tian, X., Tian, H., Tilbrook, B., Tsujino, H., Tubiello, F., Van Der Werf, G. R., Walker, A. P., Wanninkhof, R., Whitehead, C., Willstrand Wranne, A., Wright, R., Yuan, W., Yue, C., Yue, X., Zaehle, S., Zeng, J., and Zheng, B.: Global Carbon Budget 2022, Earth System Science Data, 14, 4811-4900, https://doi.org/10.5194/essd-14-4811-2022, 2022.

Frischknecht, M., Münnich, M., and Gruber, N.: Origin, Transformation, and Fate: The Three-Dimensional Biological Pump in the California Current System, Journal of Geophysical Research: Oceans, 123, 7939-7962, https://doi.org/10.1029/2018JC013934, 2018.

Gabric, A. J., Garcia, L., Van Camp, L., Nykjaer, L., Eifler, W., and Schrimpf, W.: Offshore export of shelf production in the Cape Blanc (Mauritania) giant filament as derived from coastal zone color scanner imagery, Journal of Geophysical Research: Oceans, 98, 4697-4712, https://doi.org/10.1029/92JC01714, 1993.

Gómez-Letona, M., Ramos, A. G., Coca, J., and Arístegui, J.: Trends in Primary Production in the Canary Current Upwelling System—A Regional Perspective Comparing Remote Sensing Models, Frontiers in Marine Science, Volume 4 - 2017, https://doi.org/10.3389/fmars.2017.00370, 2017.

Goudie, A. S. and Middleton, N. J.: Saharan dust storms: nature and consequences, Earth-Science Reviews, 56, 179-204, 2001.

Guerreiro, C., Cachão, M., Pawlowsky-Glahn, V., Oliveira, A., and Rodrigues, A.: Compositional Data Analysis (CoDA) as a tool to study the (paleo)ecology of coccolithophores from coastal-neritic settings off central Portugal, Sedimentary Geology, 319, 134-146, http://dx.doi.org/10.1016/j.sedgeo.2015.01.012, 2015a.

Guerreiro, C., de Stigter, H., Cachão, M., Oliveira, A., and Rodrigues, A.: Coccoliths from recent sediments of the central Portuguese margin: Taphonomical and ecological inferences, Marine Micropaleontology, 114, 55-68, http://dx.doi.org/10.1016/j.marmicro.2014.11.001, 2015b.

Guerreiro, C. V., Ziveri, P., Cavaleiro, C., and Stuut, J. B. W.: Coccolith-calcite Sr/Ca as a proxy for transient export production related to Saharan dust deposition in the tropical North Atlantic, Scientific Reports, 14, 4295, https://doi.org/10.1038/s41598-024-54001-3, 2024.

Guerreiro, C. V., Baumann, K.-H., Brummer, G.-J. A., Korte, L. F., Sá, C., and Stuut, J.-B. W.: Transatlantic gradients in calcifying phytoplankton (coccolithophore) fluxes, Progress in Oceanography, 176, 102140, https://doi.org/10.1016/j.pocean.2019.102140, 2019.

Guerreiro, C. V., Baumann, K.-H., Brummer, G.-J. A., Valente, A., Fischer, G., Ziveri, P., Brotas, V., and Stuut, J.-B. W.: Carbonate fluxes by coccolithophore species between NW Africa and the Caribbean: Implications for the biological carbon pump, Limnology and Oceanography, 66, 3190-3208, https://doi.org/10.1002/lno.11872, 2021.

Guerreiro, C. V., Baumann, K. H., Brummer, G. J. A., Fischer, G., Korte, L. F., Merkel, U., Sá, C., de Stigter, H., and Stuut, J. B. W.: Coccolithophore fluxes in the open tropical North Atlantic: influence of thermocline depth, Amazon water, and Saharan dust, Biogeosciences, 14, 4577-4599, https://doi.org/10.5194/bg-14-4577-2017, 2017.

Guerreiro, C. V., Ferreira, A., Cros, L., Stuut, J.-B., Baker, A., Tracana, A., Pinto, C., Veloso, V., Rees, A. P., Cachão, M. A. P., Nunes, T., and Brotas, V.: Response of coccolithophore communities to oceanographic and atmospheric processes across the North- and Equatorial Atlantic, Frontiers in Marine Science, 10, https://doi.org/10.3389/fmars.2023.1119488, 2023.

Guieu, C., Aumont, O., Paytan, A., Bopp, L., Law, C. S., Mahowald, N., Achterberg, E. P., Marañón, E., Salihoglu, B., Crise, A., Wagener, T., Herut, B., Desboeufs, K., Kanakidou, M., Olgun, N., Peters, F., Pulido-Villena, E., Tovar-Sanchez, A., and Völker, C.: The significance of the episodic nature of atmospheric deposition to Low Nutrient Low Chlorophyll regions, Global Biogeochemical Cycles, 28, 1179-1198, https://doi.org/10.1002/2014GB004852, 2014.

Hailegeorgis, D., Lachkar, Z., Rieper, C., and Gruber, N.: A Lagrangian study of the contribution of the Canary coastal upwelling to the nitrogen budget of the open North Atlantic, Biogeosciences, 18, 303-325, https://doi.org/10.5194/bg-18-303-2021, 2021.

Hernández-Guerra, A., Fraile-Nuez, E., López-Laatzen, F., Martínez, A., Parrilla, G., and Vélez-Belchí, P.: Canary Current and North Equatorial Current from an inverse box model, Journal of Geophysical Research: Oceans, 110, https://doi.org/10.1029/2005JC003032, 2005.

Hernández-Hernández, N., Arístegui, J., Montero, M. F., Velasco-Senovilla, E., Baltar, F., Marrero-Díaz, Á., Martínez-Marrero, A., and Rodríguez-Santana, Á.: Drivers of Plankton Distribution Across Mesoscale Eddies at Submesoscale Range, Frontiers in Marine Science, Volume 7 - 2020, https://doi.org/10.3389/fmars.2020.00667, 2020.

Hernández-Hernández, N., Santana-Falcón, Y., Montero, M. F., Benavides, M., Delgado-Huertas, A., Álvarez-Salgado, X. A., Land, P., and Arístegui, J.: Comparing *in situ* and satellite-derived primary production estimates in the Canary Current upwelling region, Journal of Marine Systems, 251, 104109, https://doi.org/10.1016/j.jmarsys.2025.104109, 2025.

Hopkins, J., Henson, S. A., Painter, S. C., Tyrrell, T., and Poulton, A. J.: Phenological characteristics of global coccolithophore blooms, Global Biogeochemical Cycles, 29, 239-253, https://doi.org/10.1002/2014GB004919, 2015.

Hosegood, P. J., Nightingale, P. D., Rees, A. P., Widdicombe, C. E., Woodward, E. M. S., Clark, D. R., and Torres, R. J.: Nutrient pumping by submesoscale circulations in the mauritanian upwelling system, Progress in Oceanography, 159, 223-236, https://doi.org/10.1016/j.pocean.2017.10.004, 2017.

Hutchins, D. A.: Forecasting the rain ratio, Nature, 476, 41-42, https://doi.org/10.1038/476041a, 2011.

Jickells, T., Boyd, P., and Hunter, K. A.: Biogeochemical Impacts of Dust on the Global Carbon Cycle, in: Mineral Dust: A Key Player in the Earth System, edited by: Knippertz, P., and Stuut, J.-B. W., Springer Netherlands, Dordrecht, 359-384, https://doi.org/10.1007/978-94-017-8978-3_14, 2014.

Jickells, T. D., Dorling, S., Deuser, W. G., Church, T. M., Arimoto, R., and Prospero, J. M.: Air-borne dust fluxes to a deep water sediment trap in the Sargasso Sea, Global Biogeochemical Cycles, 12, 311-320, https://doi.org/10.1029/97GB03368, 1998.

Formatted: Font: Italic

Jickells, T. D., An, Z. S., Andersen, K. K., Baker, A. R., Bergametti, G., Brooks, N., Cao, J. J., Boyd, P. W., Duce, R. A., Hunter, K. A., Kawahata, H., Kubilay, N., laRoche, J., Liss, P. S., Mahowald, N., Prospero, J. M., Ridgwell, A. J., Tegen, I., and Torres, R.: Global Iron Connections Between Desert Dust, Ocean Biogeochemistry, and Climate, Science, 308, 67-71, 2005.

Jönsson, B. F. and Salisbury, J. E.: Episodicity in phytoplankton dynamics in a coastal region, Geophysical Research Letters, 43, 5821-5828, https://doi.org/10.1002/2016GL068683, 2016.

Jönsson, B. F., Salisbury, J. E., and Mahadevan, A.: Extending the use and interpretation of ocean satellite data using Lagrangian modelling, International Journal of Remote Sensing, 30, 3331-3341, 10.1080/01431160802558758, 2009.

Kahru, M., Kudela, R., Manzano-Sarabia, M., and Mitchell, B. G.: Trends in primary production in the California Current detected with satellite data, Journal of Geophysical Research: Oceans, 114, https://doi.org/10.1029/2008JC004979, 2009.

Karstensen, J., Stramma, L., and Visbeck, M.: Oxygen minimum zones in the eastern tropical Atlantic and Pacific oceans, Progress in Oceanography, 77, 331-350, https://doi.org/10.1016/j.pocean.2007.05.009, 2008.

Katz, E. J.: Dynamic topography of the sea surface in the equatorial Atlantic, Journal of Marine Research, 39, 53-63, 1981.

Klenz, T., Dengler, M., and Brandt, P.: Seasonal Variability of the Mauritania Current and Hydrography at 18°N, Journal of Geophysical Research: Oceans, 123, 8122-8137, https://doi.org/10.1029/2018JC014264, 2018.

Knecht, N. S., Benedetti, F., Hofmann Elizondo, U., Bednaršek, N., Chaabane, S., de Weerd, C., Peijnenburg, K. T. C. A., Schiebel, R., and Vogt, M.: The Impact of Zooplankton Calcifiers on the Marine Carbon Cycle, Global Biogeochemical Cycles, 37, e2022GB007685, https://doi.org/10.1029/2022GB007685, 2023.

Knippertz, P. and Todd, M. C.: Mineral dust aerosols over the Sahara: Meteorological controls on emission and transport and implications for modeling, Reviews of Geophysics, 50, https://doi.org/10.1029/2011RG000362, 2012.

Koebrich, M. I., Baumann, K. H., and Fischer, G.: Seasonal and inter-annual dynamics of coccolithophore fluxes from the upwelling region off Cape Blanc, NW Africa, J. Micropalaeontol., 35, 103-116, https://doi.org/10.1144/jmpaleo2014-024, 2016.

Kok, J. F., Albani, S., Mahowald, N. M., and Ward, D. S.: An improved dust emission model – Part 2: Evaluation in the Community Earth System Model, with implications for the use of dust source functions, Atmos. Chem. Phys., 14, 13043-13061, https://doi.org/10.5194/acp-14-13043-2014, 2014.

Korte, L. F., Brummer, G.-J. A., van der Does, M., Guerreiro, C. V., Mienis, F., Munday, C. I., Ponsoni, L., Schouten, S., and Stuut, J.-B. W.: Multiple drivers of production and particle export in the western tropical North Atlantic, Limnology and Oceanography, 65, 2108-2124, https://doi.org/10.1002/lno.11442, 2020.

Korte, L. F., Brummer, G. J. A., van der Does, M., Guerreiro, C. V., Hennekam, R., van Hateren, J. A., Jong, D., Munday, C. I., Schouten, S., and Stuut, J. B. W.: Downward particle fluxes of biogenic matter and Saharan dust across the equatorial North Atlantic, Atmos. Chem. Phys., 17, 6023-6040, https://doi.org/10.5194/acp-17-6023-2017, 2017.

Kostianoy, A. G. and Zatsepin, A. G.: The West African coastal upwelling filaments and cross-frontal water exchange conditioned by them, Journal of Marine Systems, 7, 349-359, https://doi.org/10.1016/0924-7963(95)00029-1, 1996.

Lathuilière, C., Echevin, V., and Lévy, M.: Seasonal and intraseasonal surface chlorophyll-a variability along the northwest African coast, Journal of Geophysical Research: Oceans, 113, https://doi.org/10.1029/2007JC004433, 2008.

Lellouche, J. M., Greiner, E., Le Galloudec, O., Garric, G., Regnier, C., Drevillon, M., Benkiran, M., Testut, C. E., Bourdalle-Badie, R., Gasparin, F., Hernandez, O., Levier, B., Drillet, Y., Remy, E., and Le Traon, P. Y.: Recent updates to the Copernicus Marine Service global ocean monitoring and forecasting real-time 1⁄12° high-resolution system, Ocean Sci., 14, 1093-1126, https://doi.org/10.5194/os-14-1093-2018, 2018.

Longhurst, A. R.: Ecological geography of the sea (2nd edition), Academic Press, San Diego, 542 pp.2006.

Lovecchio, E., Gruber, N., and Münnich, M.: Mesoscale contribution to the long-range offshore transport of organic carbon from the Canary Upwelling System to the open North Atlantic, Biogeosciences, 15, 5061-5091, https://doi.org/10.5194/bg-15-5061-2018, 2018.

Mann, K. H. and Lazier, J. P.: Dynamics of marine ecosystems, biological-physical interactions in the oceans (3rd edition), Blackwell, Malden, USA, Oxford, UK2006.

Mark Moore, C., Mills, M. M., Achterberg, E. P., Geider, R. J., LaRoche, J., Lucas, M. I., McDonagh, E. L., Pan, X., Poulton, A. J., Rijkenberg, M. J. A., Suggett, D. J., Ussher, S. J., and Woodward, E. M. S.: Large-scale distribution of Atlantic nitrogen fixation controlled by iron availability, Nature Geosci, 2, 867-871, https://doi.org/10.1038/ngeo667, 2009.

Marrero-Betancort, N., Marcello, J., Rodríguez Esparragón, D., and Hernández-León, S.: Wind variability in the Canary Current during the last 70 years, Ocean Sci., 16, 951-963, https://doi.org/10.5194/os-16-951-2020, 2020.

Measures, C. I., Landing, W. M., Brown, M. T., and Buck, C. S.: High-resolution Al and Fe data from the Atlantic Ocean CLIVAR-CO2 Repeat Hydrography A16N transect: Extensive linkages between atmospheric dust and upper ocean geochemistry, Global Biogeochemical Cycles, 22, https://doi.org/10.1029/2007GB003042, 2008.

Merle, J.: Seasonal Heat Budget in the Equatorial Atlantic Ocean, Journal of Physical Oceanography, 10, 464-469, https://doi.org/10.1175/1520-0485(1980)010<0464:SHBITE>2.0.CO;2, 1980a.

Merle, J.: Seasonal-variation of heat-storage in the tropical atlantic-ocean, Oceanologica Acta, 3, 455-463, 1980b.

Messié, M. and Chavez, F. P.: Seasonal regulation of primary production in eastern boundary upwelling systems, Progress in Oceanography, 134, 1-18, https://doi.org/10.1016/j.pocean.2014.10.011, 2015.

Meunier, T., Barton, E. D., Barreiro, B., and Torres, R.: Upwelling filaments off Cap Blanc: Interaction of the NW African upwelling current and the Cape Verde frontal zone eddy field?, Journal of Geophysical Research: Oceans, 117, https://doi.org/10.1029/2012JC007905, 2012.

Milliman, J. D.: Production and accumulation of calcium carbonate in the ocean: Budget of a nonsteady state, Global Biogeochemical Cycles, 7, 927-957, https://doi.org/10.1029/93GB02524, 1993.

Morel, A.: Light and marine photosynthesis: a spectral model with geochemical and climatological implications, Progress in Oceanography, 26, 263-306, https://doi.org/10.1016/0079-6611(91)90004-6, 1991.

Okin, G. S., Baker, A. R., Tegen, I., Mahowald, N. M., Dentener, F. J., Duce, R. A., Galloway, J. N., Hunter, K., Kanakidou, M., Kubilay, N., Prospero, J. M., Sarin, M., Surapipith, V., Uematsu, M., and Zhu, T.: Impacts of atmospheric nutrient deposition on marine productivity: Roles of nitrogen, phosphorus, and iron, Global Biogeochemical Cycles, 25, https://doi.org/10.1029/2010GB003858, 2011.

Oschlies, A. and Garçon, V.: Eddy-induced enhancement of primary production in a model of the North Atlantic Ocean, Nature, 394, 266-269, https://doi.org/10.1038/28373, 1998.

Pabortsava, K., Lampitt, R. S., Benson, J., Crowe, C., McLachlan, R., Le Moigne, F. A. C., Mark Moore, C., Pebody, C., Provost, P., Rees, A. P., Tilstone, G. H., and Woodward, E. M. S.: Carbon sequestration in the deep Atlantic enhanced by Saharan dust, Nature Geosci, 10, 189-194, https://doi.org/10.1038/ngeo2899, 2017.

Pastor, M. V., Palter, J. B., Pelegrí, J. L., and Dunne, J. P.: Physical drivers of interannual chlorophyll variability in the eastern subtropical North Atlantic, Journal of Geophysical Research: Oceans, 118, 3871-3886, https://doi.org/10.1002/jgrc.20254, 2013.

Pastor, M. V., Peña-Izquierdo, J., Pelegrí, J. L., and Marrero-Díaz, Á.: Meridional changes in water mass distributions off NW Africa during November 2007/2008, Ciencias Marinas, 38, 223-244, https://doi.org/10.7773/cm.v38i1B.1831, 2011.

Pastor, M. V., Pelegrí, J. L., Hernández-Guerra, A., Font, J., Salat, J., and Emelianov, M.: Water and nutrient fluxes off Northwest Africa, Continental Shelf Research, 28, 915-936, https://doi.org/10.1016/j.csr.2008.01.011, 2008.

Pelegrí, J. L., Peña-Izquierdo, J., Machín, F., Meiners, C., and Presas-Navarro, C.: Oceanography of the Cape Verde Basin and Mauritanian Slope Waters, in: Deep-Sea Ecosystems Off Mauritania: Research of Marine Biodiversity and Habitats in the Northwest African Margin, edited by: Ramos, A., Ramil, F., and Sanz, J. L., Springer Netherlands, Dordrecht, 119-153, https://doi.org/10.1007/978-94-024-1023-5_3, 2017.

Pelegrí, J. L., Arístegui, J., Cana, L., González-Dávila, M., Hernández-Guerra, A., Hernández-León, S., Marrero-Díaz, A., Montero, M. F., Sangrà, P., and Santana-Casiano, M.: Coupling between the open ocean and the coastal upwelling region off northwest Africa: water recirculation and offshore pumping of organic matter, Journal of Marine Systems, 54, 3-37, https://doi.org/10.1016/j.jmarsys.2004.07.003, 2005.

Philander, S. G.: Atlantic Ocean Equatorial Currents*, in: Encyclopedia of Ocean Sciences (Second Edition), edited by: Steele, J. H., Academic Press, Oxford, 234-237, https://doi.org/10.1016/B978-012374473-9.00361-1, 2001.

Polonsky, A. B. and Serebrennikov, A. N.: Long-Term Sea Surface Temperature Trends in the Canary Upwelling Zone and their Causes, Izvestiya, Atmospheric and Oceanic Physics, 54, 1062-1067, https://doi.org/10.1134/S0001433818090281, 2018.

Poulton, A. J., Holligan, P. M., Hickman, A., Kim, Y.-N., Adey, T. R., Stinchcombe, M. C., Holeton, C., Root, S., and Woodward, E. M. S.: Phytoplankton carbon fixation, chlorophyll-biomass and diagnostic pigments in the Atlantic Ocean, Deep Sea Research Part II: Topical Studies in Oceanography, 53, 1593-1610, https://doi.org/10.1016/j.dsr2.2006.05.007, 2006.

Powell, C. F., Baker, A. R., Jickells, T. D., Bange, H. W., Chance, R. J., and Yodle, C.: Estimation of the Atmospheric Flux of Nutrients and Trace Metals to the Eastern Tropical North Atlantic Ocean, Journal of the Atmospheric Sciences, 72, 4029-4045, https://doi.org/10.1175/JAS-D-15-0011.1, 2015.

Prospero, J. M. and Carlson, T. N.: Vertical and areal distribution of Saharan dust over the western equatorial north Atlantic Ocean, Journal of Geophysical Research (1896-1977), 77, 5255-5265, https://doi.org/10.1029/JC077i027p05255, 1972.

Prospero, J. M., Collard, F.-X., Molinié, J., and Jeannot, A.: Characterizing the annual cycle of African dust transport to the Caribbean Basin and South America and its impact on the environment and air quality, Global Biogeochemical Cycles, 28, 757-773, https://doi.org/10.1002/2013GB004802, 2014.

Reid, J. L.: On the total geostrophic circulation of the North Atlantic Ocean: Flow patterns, tracers, and transports, Progress in Oceanography, 33, 1-92, https://doi.org/10.1016/0079-6611(94)90014-0, 1994.

Romero, O. E., Baumann, K. H., Zonneveld, K. A. F., Donner, B., Hefter, J., Hamady, B., Pospelova, V., and Fischer, G.: Flux variability of phyto- and zooplankton communities in the Mauritanian coastal upwelling between 2003 and 2008, Biogeosciences, 17, 187-214, https://doi.org/10.5194/bg-17-187-2020, 2020.

Sangrà, P., Pascual, A., Rodríguez-Santana, Á., Machín, F., Mason, E., McWilliams, J. C., Pelegrí, J. L., Dong, C., Rubio, A., Arístegui, J., Marrero-Díaz, Á., Hernández-Guerra, A., Martínez-Marrero, A., and Auladell, M.: The Canary Eddy Corridor: A major pathway for long-lived eddies in the subtropical North Atlantic, Deep Sea Research Part I: Oceanographic Research Papers, 56, 2100-2114, https://doi.org/10.1016/j.dsr.2009.08.008, 2009.

Santana-Falcón, Y., Mason, E., and Arístegui, J.: Offshore transport of organic carbon by upwelling filaments in the Canary Current System, Progress in Oceanography, 186, 102322, https://doi.org/10.1016/j.pocean.2020.102322, 2020.

Siedler, G., Zangenberg, N., Onken, R., and Morlière, A.: Seasonal changes in the tropical Atlantic circulation: Observation and simulation of the Guinea Dome, Journal of Geophysical Research: Oceans, 97, 703-715, https://doi.org/10.1029/91JC02501, 1992.

Siemer, J. P., Machín, F., González-Vega, A., Arrieta, J. M., Gutiérrez-Guerra, M. A., Pérez-Hernández, M. D., Vélez-Belchí, P., Hernández-Guerra, A., and Fraile-Nuez, E.: Recent Trends in SST, Chl-*a*, Productivity and Wind Stress in Upwelling and Open Ocean Areas in the Upper Eastern North Atlantic Subtropical Gyre, Journal of Geophysical Research: Oceans, 126, e2021JC017268, https://doi.org/10.1029/2021JC017268, 2021.

Signorini, S. R., Franz, B. A., and McClain, C. R.: Chlorophyll variability in the oligotrophic gyres: mechanisms, seasonality and trends, Frontiers in Marine Science, Volume 2 - 2015, https://doi.org/10.3389/fmars.2015.00001, 2015.

Skonieczny, C., Bory, A., Bout-Roumazeilles, V., Abouchami, W., Galer, S. J. G., Crosta, X., Diallo, A., and Ndiaye, T.: A three-year time series of mineral dust deposits on the West African margin: Sedimentological and geochemical signatures and implications for interpretation of marine paleo-dust records, Earth and Planetary Science Letters, 364, 145-156, http://dx.doi.org/10.1016/j.epsl.2012.12.039, 2013.

Sprengel, C., Baumann, K.-H., Henderiks, J., Henrich, R., and Neuer, S.: Modern coccolithophore and carbonate sedimentation along a productivity gradient in the Canary Islands region: seasonal export production and surface accumulation rates, Deep Sea Research Part II: Topical Studies in Oceanography, 49, 3577-3598, https://doi.org/10.1016/S0967-0645(02)00099-1, 2002.

Stramma, L. and England, M.: On the water masses and mean circulation of the South Atlantic Ocean, Journal of Geophysical Research C: Oceans, 104, 20863-20883, 1999.

Formatted: Font: Italic

Stramma, L. and Schott, F.: The mean flow field of the tropical Atlantic Ocean, Deep Sea Research Part II: Topical Studies in Oceanography, 46, 279-303, https://doi.org/10.1016/S0967-0645(98)00109-X, 1999.

Stuut, J.-B. W. and Cruise participants: Cruise report and preliminary results RV Pelagia expedition 64PE378 TRAFFIC II, NIOZ - Royal Netherlands Institute for Sea Research, Texel, 54, 2013.

Stuut, J.-B. W. and Cruise participants: Cruise report and preliminary results RV Pelagia expedition 64PE514 DUST 2023, NIOZ - Royal Netherlands Institute for Sea Research, Texel, 51, 2023.

Stuut, J.-B. W., Zabel, M., Ratmeyer, V., Helmke, P., Schefuß, E., Lavik, G., and Schneider, R. R.: Provenance of present-day eolian dust collected off NW Africa, Journal of Geophysical Research, 110, https://doi.org/doi:10.1029/2004JD005161, 10.1029/2004JD005161, 2005.

Tilstone, G. H., Xie, Y.-y., Robinson, C., Serret, P., Raitsos, D. E., Powell, T., Aranguren-Gassis, M., Garcia-Martin, E. E., and Kitidis, V.: Satellite estimates of net community production indicate predominance of net autotrophy in the Atlantic Ocean, Remote Sensing of Environment, 164, 254-269, https://doi.org/10.1016/j.rse.2015.03.017, 2015.

Tsamalis, C., Chédin, A., Pelon, J., and Capelle, V.: The seasonal vertical distribution of the Saharan Air Layer and its modulation by the wind, Atmos. Chem. Phys., 13, 11235-11257, https://doi.org/10.5194/acp-13-11235-2013, 2013.

Ussher, S. J., Achterberg, E. P., Powell, C., Baker, A. R., Jickells, T. D., Torres, R., and Worsfold, P. J.: Impact of atmospheric deposition on the contrasting iron biogeochemistry of the North and South Atlantic Ocean, Global Biogeochemical Cycles, 27, 1096-1107, https://doi.org/10.1002/gbc.20056, 2013.

Van Camp, L., Nykjaer, L., Mittelstaedt, E., and Schlittenhardt, P.: Upwelling and boundary circulation off Northwest Africa as depicted by infrared and visible satellite observations, Progress in Oceanography, 26, 357-402, https://doi.org/10.1016/0079-6611(91)90012-B, 1991.

Van der Does, M., Brummer, G.-J. A., Korte, L. F., and Stuut, J.-B. W.: Seasonality in Saharan Dust Across the Atlantic Ocean: From Atmospheric Transport to Seafloor Deposition, Journal of Geophysical Research: Atmospheres, 126, e2021JD034614, https://doi.org/10.1029/2021JD034614, 2021.

Van der Does, M., Korte, L. F., Munday, C. I., Brummer, G. J. A., and Stuut, J. B. W.: Particle size traces modern Saharan dust transport and deposition across the equatorial North Atlantic, Atmos. Chem. Phys., 16, 13697-13710, https://doi.org/10.5194/acp-16-13697-2016, 2016.

Van der Does, M., Brummer, G.-J. A., van Crimpen, F. C. J., Korte, L. F., Mahowald, N. M., Merkel, U., Yu, H., Zuidema, P., and Stuut, J.-B. W.: Tropical rains controlling deposition of Saharan dust across the North Atlantic Ocean, Geophysical Research Letters, 47, 1-10, https://doi.org/10.1029/2019GL086867, 2020.

Van der Jagt, H., Friese, C. A., Stuut, J.-B. W., Fischer, G., and Iversen, M. H.: The ballasting effect of Saharan dust deposition on aggregate dynamics and carbon export: aggregation, settling and scavenging of marine snow, Limnology & Oceanography, 63, 1386-1394, https://doi.org/10.1002/lno.10779, 2018.

Varela, R., Álvarez, I., Santos, F., deCastro, M., and Gómez-Gesteira, M.: Has upwelling strengthened along worldwide coasts over 1982-2010?, Scientific Reports, 5, 10016, https://doi.org/10.1038/srep10016, 2015.

Vazquez, R., Parras-Berrocal, I., Cabos, W., Sein, D. V., Mañanes, R., and Izquierdo, A.: Assessment of the Canary current upwelling system in a regionally coupled climate model, Climate Dynamics, 58, 69-85, https://doi.org/10.1007/s00382-021-05890-x, 2022.

Waniek, J. J., Koeve, W., and Prien, R. D.: Trajectories of sinking particles and the catchment areas above sediment traps in the northeast Atlantic, Journal of Marine Research, 58, 983-1006, 2000.

Wefer, G. and Fischer, G.: Seasonal patterns of vertical particle flux in equatorial and coastal upwelling areas of the eastern Atlantic, Deep Sea Research Part I: Oceanographic Research Papers, 40, 1613-1645, https://doi.org/10.1016/0967-0637(93)90019-Y, 1993.

Wilken, S., Huisman, J., Naus-Wiezer, S., and Van Donk, E.: Mixotrophic organisms become more heterotrophic with rising temperature, Ecology Letters, 16, 225-233, https://doi.org/10.1111/ele.12033, 2013.

Yu, H., Tan, Q., Chin, M., Remer, L. A., Kahn, R. A., Bian, H., Kim, D., Zhang, Z., Yuan, T., Omar, A. H., Winker, D. M., Levy, R. C., Kalashnikova, O., Crepeau, L., Capelle, V., and Chédin, A.: Estimates of African Dust Deposition Along the Trans-Atlantic Transit Using the Decadelong Record of Aerosol Measurements from CALIOP, MODIS, MISR, and IASI, Journal of Geophysical Research: Atmospheres, 124, 7975-7996, https://doi.org/10.1029/2019jd030574, 2019.

Zenk, W., Klein, B., and Schroder, M.: Cape Verde Frontal Zone, Deep Sea Research Part A. Oceanographic Research Papers, 38, S505-S530, https://doi.org/10.1016/S0198-0149(12)80022-7, 1991.

Zhan, W., Feng, M., Zhang, Y., Shen, X., Zhan, H., and He, Q.: Reduced and smaller phytoplankton during marine heatwaves in eastern boundary upwelling systems, Communications Earth & Environment, 5, 629, https://doi.org/10.1038/s43247-024-01805-w, 2024.

Formatted: English (UK)

Page 13: [1] Deleted	**Catarina V. Guerreiro**	**14/05/2026 11:12:00**
Page 15: [2] Deleted	**Catarina V. Guerreiro**	**24/05/2026 20:21:00**
Page 18: [3] Deleted	**Catarina V. Guerreiro**	**16/05/2026 20:52:00**
Page 24: [4] Deleted	**Catarina V. Guerreiro**	**16/05/2026 23:33:00**